D. Invernizzi, L. Dozio
A Fully Consistent Linearized Model for Vibration Analysis of Rotating Beams in the Framework of Geometrically Exact Theory
Journal of Sound and Vibration, Vol. 370, 2016, p. 351-371
doi:10.1016/j.jsv.2016.01.049

A fully consistent linearized model for vibration analysis of rotating beams in the framework of geometrically exact theory

Davide Invernizzi[a,1], Lorenzo Dozio[a,2,*]

[a] *Department of Aerospace Science and Technology, Politecnico di Milano, via La Masa, 34, 20156 Milano, Italy*

Abstract

The equations of motions governing the free vibrations of prismatic slender beams rotating in a plane at constant angular velocity are derived according to a geometrically exact approach. Compared to other modeling methods, additional stiffening terms induced by pre-stress are found in the dynamic equations after fully consistent linearization about the deformed equilibrium configuration. These terms include axial, bending and torsional stiffening effects which arise when second-order generalized strains are retained. It is shown that their contribution becomes relevant at moderate to high angular speeds, where high means that the equilibrium state is subject to strains close to the limit where a physically linear constitutive law still applies. In particular, the importance of the axial stiffening is specifically investigated. The natural frequencies as a function of the angular velocity and other system parameters are computed and compared with benchmark cases available in the literature. Finally, the error on the modal characteristics of the rotating beam is evaluated when the linearization is carried out about the undeformed configuration.

Keywords: rotating beam, geometrically exact beam theory, free vibration, geometric stiffening, consistent linearization

1. Introduction

The modeling of elastic bodies undergoing large rotational motion has been widely studied since the sixties, when it became necessary to take into account the flexibility of the components in order to perform more accurate simulations and design lighter and more efficient structures. Beams, due to their importance in many engineering applications and their intrinsic simplicity, have received a particular attention. During the last four decades, several authors proposed different mathematical models with the aim of correctly estimating the modal characteristics and dynamic response of rotating flexible beams. Most studies come

*Corresponding author
Email addresses: davide.invernizzi@polimi.it (Davide Invernizzi), lorenzo.dozio@polimi.it (Lorenzo Dozio)
[1] PhD student.
[2] Associate Professor.

from researchers working in the aerospace field since rotating beams can be often used as a simple model for propellers, helicopter blades, turbine blades and satellite booms.

Owing to the huge amount of papers published on this topic, a comprehensive survey of the subject is beyond the scope of this paper. Some excellent reviews can be found in the related literature, which are extremely useful in identifying and tracking the major developments over a large span of time and can be also helpful in locating the contribution of the present work. In particular, the reader is referred to the review papers of Sharf [30] and Kunz [16], which cover most of the material up to the mid-nineties. An extensive overview of the most recent material can be found in the book of Hodges [10].

It is well known that, even though a flexible beam undergoes small elastic vibrations during rotation, several motion-induced stiffness terms can be missed in those formulations where linear strain quantities relative to a floating frame following the rotation of the beam are early adopted in the expression of the total potential energy of the system. This simplified scheme, which leads to linear models characterized by a spurious loss of bending rigidity, in the literature is often referred to as premature or inconsistent linearization of the deformation field during the derivation of the equations of motion (Mayo et al. [22]).

One of the first attempts to account for motion-induced stiffening dates back to the paper of Houbolt and Brooks [12] in which a set of equations governing the coupled torsion-bending vibrations were derived for a twisted rotating beam. The linearization was retarded as much as possible to include all the first-order terms arising from the coupling between the tensile load induced by the centrifugal acceleration and the other strain measures.

Some years later, a similar approach was followed by Likins et al. [19], who derived the linear equations governing the out-of-plane transverse vibrations of spinning elastic bodies by accounting for the potential energy resulting from the centrifugal force. By neglecting the axial vibrations, they also discarded the gyroscopic coupling between the axial and bending motion due to the Coriolis acceleration, which instead is relevant as the angular velocity increases as shown by Yoo and Shin [36].

Vigneron [33] followed similar steps in deriving the linearized dynamic equations of rotating beams but he divided explicitly the axial displacement into one contribution due to the stretching of the beam elastic axis and another contribution related to the so-called foreshortening effect. In this way, the geometric stiffening effect appears in the kinetic energy associated with the foreshortening displacement component. This approach has strong similarities with the one proposed by Kane et al. [14], also known as *"foreshortening approach"*, which is based on a hybrid set of deformation variables involving both non-Cartesian (stretch deformation) and classical Cartesian variables (transverse deformation). The use of the principle of virtual work combined with the stretch variable substitution yields a motion-induced stiffening contribution due to the work done by the inertial and external forces for that part of the virtual displacement related to foreshortening. When linearized equations are sought for, this method is equivalent to those classical formulations which include the elastic potential energy resulting from the centrifugal force (Meirovitch [23], Yardimoglu

and Inman [35], Banerjee and Kennedy [3]).

A different approach was followed by Laskin et al. [18] and later by Lin and Hsiao [20], Huang et al. [13] and Kim et al. [15], who decomposed the beam axial displacement into a small but finite quasi-static component, computed before solving the equations of motions, and an infinitesimal transient component. This method allows to include the effect of the deformed geometry, which has a simple analytical solution for a beam rotating in a plane. However, as shown in the following, they do not foresee several stiffening terms, which should arise from the corresponding nonlinear term in the Green-Lagrange strain. This leads to the wrong prediction of a critical value of the angular velocity where the model exhibits an instability also for stiffening materials.

Another interesting study was presented by Banerjee and Dickens [2], in which a consistent linearization procedure was exploited to include several motion-induced stiffness terms for a generic deformable body in large overall motion. The work of the zeroth-order components of the stress tensor for the nonlinear part of the virtual variation of the Green-Lagrange tensor was retained in the formulation and allows to capture some geometric stiffening components, although the authors did not provide the equations for the case of a rotating beam.

A more modern and rigorous approach of modeling rotating beams is based on the geometrically exact theory. The literature on geometrically-exact beam theories (GEBTs) dates back to the seminal work of Reissner [28], where a large strain theory was first presented and later extended to the case of spatially curved beams and large displacements [29]. The kinematics of the geometrically exact beam was first introduced by Simo [31], but similar developments can be found in Borri and Merlini [4] and Cardona and Geradin [5]. In particular, the novelty of these works relies in the exact treatment of the orientation of the beam cross section. In Danielson and Hodges [6], the three-dimensional strain field has been written in terms of the intrinsic one-dimensional measures for initially twisted and curved beams. Hodges [9] has also derived a mixed variational formulation for the dynamics of moving beams which can be used once appropriate constitutive laws and kinematics relations are provided.

A solid and comprehensive theoretical background to the geometrically exact approach appeared about one decade ago in the books of Hodges [10] and Pai [24]. In the first monograph, the author presents the intrinsic formulation of the dynamic equations of initially curved and twisted beams. The cross-section analysis of the beam is also discussed extensively based on the variational asymptotic method [10]. The fully intrinsic approach, since it is devoid of displacement and rotation variables, is particularly attractive to overcome the issues associated with finite rotation variables. The modeling of highly flexible structures is the main subject of the book of Pai [24], where a general displacement-based formulation of geometrically exact beams, plates and shells accounting for shear deformations and warping effects is developed.

GEBTs are based on an exact description of the beam kinematics as a one-dimensional continuum and they rely on the definition of generalized strain measures, namely the *force* and *moment* strains. Most of

these theories exploit Jaumann strains under the small strains and local rotation assumption, according to which second-order generalized strain components are neglected. The importance of these second-order terms in modeling rotating blades was highlighted by Masarati and Morandini [21] and Hodges [10], in particular for what concerns the torsional stiffening induced by a tensile load, the so-called trapeze effect. In a very recent paper, Pai [25] outlines several other problems and shortcomings present in the existing geometrically exact approaches, mainly connected to the choice of the parametrization of the orientation. Other significant contributions on the subject can be found in the work of Lacarbonara et al. [17], in which the equations of motion for unshearable rotating beams are presented. The approach was later extended to composite blades in Ref. [1].

In the present work, a geometrically exact approach is adopted to describe the kinematics of slender prismatic beams rotating in a plane at constant angular velocity. Indeed, it allows to properly include the effect of geometric nonlinearities in a systematic and straightforward manner. A linearized model is then derived for small perturbations around the equilibrium condition, which is expressed in an analytical closed form under the assumption of a physically linear constitutive law. According to the Lagrangian formulation, all the geometric stiffness terms are consistently included in the linearized equation of motions by expanding up to the second-order the strain measures. Compared to other modeling approaches available in the literature, the present formulation includes additional terms arising from second-order generalized strains, in particular axial and torsional stiffening terms. The latter contribution is the aforementioned trapeze effect, which has been already highlighted and investigated by Hodges [10]. In this work, it is shown that also the axial stiffening terms can be relevant, especially as the angular speed of the beam takes moderate to high values. The angular velocity is here considered to be high when the equilibrium condition of the rotating beam is subject to axial strain close to the limit region where a solution based on a physically linear constitutive law (i.e., small strain behavior) begins to diverge from that corresponding to a physically nonlinear law (i.e., large strain behavior).

Although the model is developed to study free vibration of isotropic slender beams, the present approach does not discard dynamic terms due to rotary inertia. It is known that the contribution due to transverse shear deformation and rotary inertia on the dynamic characteristics is comparable for non-rotating beams. However, the influence of rotary inertia can become significant even for slender beams when gyroscopic effects are introduced by the rotation (Pai et al. [26]). It will be shown in the following that several terms connected to rotary inertia are present in the equations of motion and their expression and contribution will be discussed.

The set of linearized equations for the rotating beam are derived in the form of a standard quadratic eigenvalue problem by means of the Ritz-Galerkin method. A comprehensive numerical analysis is performed in order to validate the current formulation and highlight the main differences with previous modeling approaches.

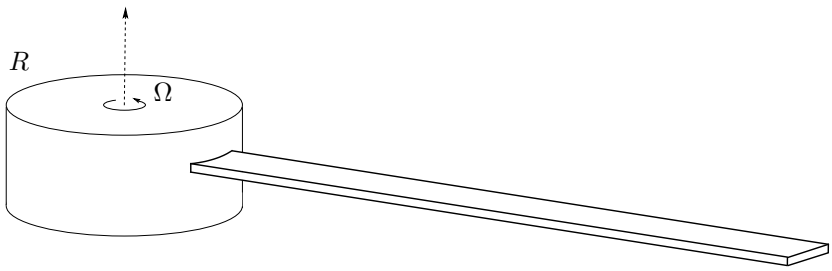

Figure 1: Cantilever prismatic beam of length ℓ attached to a rigid hub of radius R rotating at angular velocity Ω.

2. Problem statement: kinematics, strain field and principle of virtual work for a planar rotating slender beam

The system under investigation is a homogeneous cantilever flexible beam of length ℓ attached to a rigid hub of radius R freely rotating at constant angular velocity Ω (see Figure 1). The beam is assumed to be straight in the initial (undeformed) configuration, with a uniform doubly symmetric solid cross-section A made of linear elastic isotropic material of mass density ρ and Young's modulus E. Furthermore, a beam having a relatively high slenderness ratio is considered so that an unshearable 1-D model can be reasonably assumed.

In this section, the kinematics, strain field and principle of virtual work for the rotating beam are presented in the framework of the geometrically exact theory. Subsequently, the solution of the equilibrium configuration is discussed in details. Finally, the set of partial differential equations describing the free vibrations of the rotating beam for the axial, chordwise (bending in the x-y plane), flapwise (bending in the x-z plane) and torsional motions is derived from the consistent linearization of the principle of virtual work about the equilibrium state obtained before.

2.1. Kinematics of the geometrically exact beam

According to Figure 2, the motion of the elastic beam is referred to the inertial frame I ($\mathbf{i}_1$, $\mathbf{i}_2$, $\mathbf{i}_3$). The undeformed beam geometry is described by the frame B ($\mathbf{b}_1$, $\mathbf{b}_2$, $\mathbf{b}_3$). Here, $\mathbf{b}_1$ is in the direction of the centroidal axis of the undeformed beam, whereas $\mathbf{b}_2$ and $\mathbf{b}_3$ define the plane of the cross-section and give the directions of the principal axes of inertia. The position vector of the undeformed reference configuration can be written as

$$\mathbf{X} = \mathbf{X}_0 + \boldsymbol{\xi}_0 \tag{1}$$

where $\mathbf{X}_0 = (R + x)\mathbf{b}_1$ and $\boldsymbol{\xi}_0 = y\mathbf{b}_2 + z\mathbf{b}_3$. Under the assumption of cross-sections remaining plane and undeformed in their plane during the motion, i.e., in-plane and out-of-plane warpings are neglected, a local orthogonal frame T ($\mathbf{t}_1$, $\mathbf{t}_2$, $\mathbf{t}_3$) is introduced, which identifies the deformed beam geometry. Similarly to frame B, $\mathbf{t}_2$ and $\mathbf{t}_3$ lay parallel to the current cross-section of the beam and point to the direction of the

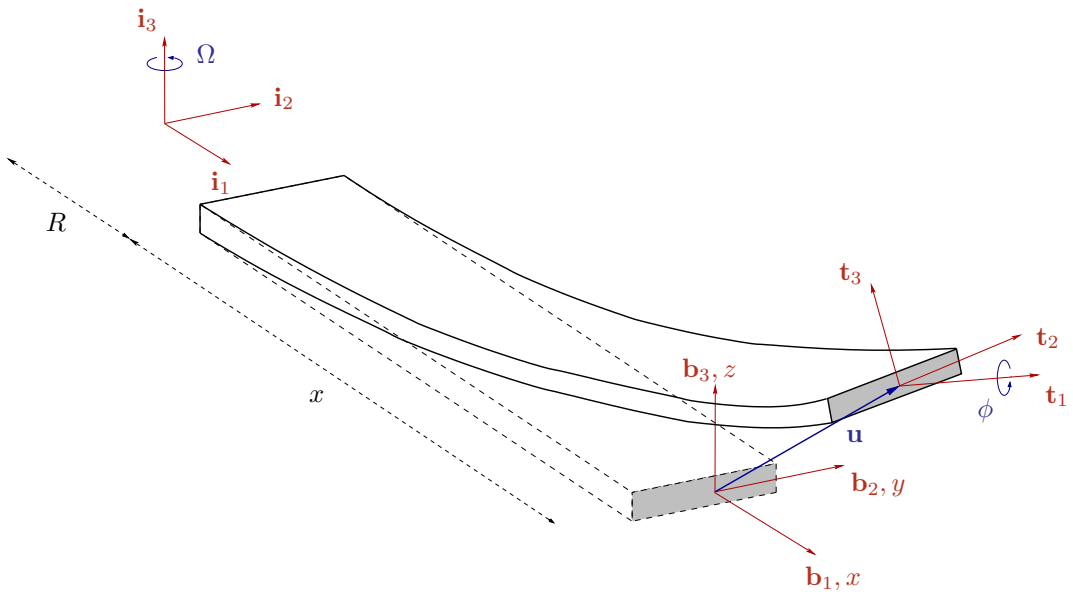

Figure 2: Definition of the reference frames.

principal axis of inertia, while $\mathbf{t}_1$ is normal to the plane of the cross-section. Frames B and T are assumed to be coincident at the initial stage. Accordingly, the position vector $\mathbf{x}$ of a generic point P of the deformed beam with respect to the inertial frame I is given by

$$\mathbf{x} = (R + x)\mathbf{b}_1 + \mathbf{u} + \boldsymbol{\xi} \tag{2}$$

where $\mathbf{u}(x,t) = u\mathbf{b}_1 + v\mathbf{b}_2 + w\mathbf{b}_3$ is the displacement vector whose components are regarded as the cross-section translation degrees of freedom, $\boldsymbol{\xi} = y\mathbf{t}_2 + z\mathbf{t}_3 = \mathbf{R} \cdot \boldsymbol{\xi}_0$, and $\mathbf{R} = \mathbf{t}_i \otimes \mathbf{b}_i$ is the rigid rotation tensor of the cross-section. They describe the fact that the cross-section rigidly moves from the reference to the current configuration.

Since the system is rotating at a constant angular velocity $\Omega\mathbf{i}_3$, the velocity and acceleration of P at time t are given, respectively, by

$$\mathbf{v} = \Omega(R + x)\mathbf{b}_2 + \Omega\mathbf{i}_3 \times (\mathbf{u} + \boldsymbol{\xi}) + \dot{\mathbf{u}} + \boldsymbol{\omega} \times \boldsymbol{\xi} \tag{3}$$

$$\mathbf{a} = -\Omega^2(R + x)\mathbf{b}_1 + \Omega\mathbf{i}_3 \times \Omega\mathbf{i}_3 \times (\mathbf{u} + \boldsymbol{\xi}) + 2\Omega\mathbf{i}_3 \times (\dot{\mathbf{u}} + \boldsymbol{\omega} \times \boldsymbol{\xi}) + \ddot{\mathbf{u}} + \dot{\boldsymbol{\omega}} \times \boldsymbol{\xi} + \boldsymbol{\omega} \times (\boldsymbol{\omega} \times \boldsymbol{\xi}) \tag{4}$$

where $\boldsymbol{\omega} = \omega_1\mathbf{t}_1 + \omega_2\mathbf{t}_2 + \omega_3\mathbf{t}_3$ is the angular velocity vector of the beam cross-section.

The overall motion is assumed to be prescribed, so that an arbitrary and kinematically admissible virtual displacement field can be written as follows

$$\delta\mathbf{x} = \delta\mathbf{u} + \boldsymbol{\delta\theta} \times \boldsymbol{\xi} \tag{5}$$

where $\boldsymbol{\delta\theta}$ is the virtual rotation vector.

Many different rotation angles can be chosen to describe the rotation of the undeformed basis vectors $\mathbf{b}_i$ to the vectors $\mathbf{t}_i$ of the deformed configuration. In this work, the following rotating matrix is used (see Ref. [24]):

$$\mathbf{R} = \begin{bmatrix} 1 & 0 & 0 \\ 0 & \cos\phi & \sin\phi \\ 0 & -\sin\phi & \cos\phi \end{bmatrix} \begin{bmatrix} R_{11} & R_{12} & R_{13} \\ -R_{12} & R_{11}+R_{13}^2/(1+R_{11}) & -R_{12}R_{13}/(1+R_{11}) \\ -R_{13} & -R_{12}R_{13}/(1+R_{11}) & R_{11}+R_{12}^2/(1+R_{11}) \end{bmatrix} \tag{6}$$

where ϕ is the twist angle with respect to the deformed axis $\mathbf{t}_1$, and

$$\begin{aligned} R_{11} &= \frac{1+\partial u/\partial x}{1+e} \\ R_{12} &= \frac{\partial v/\partial x}{1+e} \\ R_{13} &= \frac{\partial w/\partial x}{1+e} \end{aligned} \tag{7}$$

with e being the strain of the beam axis, which is expressed in terms of displacement variables as

$$e = \sqrt{\left(1+\frac{\partial u}{\partial x}\right)^2 + \left(\frac{\partial v}{\partial x}\right)^2 + \left(\frac{\partial w}{\partial x}\right)^2} - 1 \tag{8}$$

Note that the matrix in Eq. (6) is a function only of the twist angle ϕ and the displacements (u, v, w) of the beam axis, in agreement with the orthonormality condition. The above choice is considered to be appropriate for the analysis of beam-like structures undergoing weakly nonlinear elastic deformations [24].

The virtual rotation vector $\boldsymbol{\delta\theta}$ and the angular velocity $\boldsymbol{\omega}$ are resolved in the current frame T in terms of the components of the rotation matrix as follows

$$\delta\theta_1 = \delta R_{2i} R_{3i} \qquad \delta\theta_2 = -\delta R_{1i} R_{3i} \qquad \delta\theta_3 = \delta R_{1i} R_{2i} \tag{9}$$

$$\omega_1 = \frac{\partial R_{2i}}{\partial t} R_{3i} \qquad \omega_2 = -\frac{\partial R_{1i}}{\partial t} R_{3i} \qquad \omega_3 = \frac{\partial R_{1i}}{\partial t} R_{2i} \tag{10}$$

where the summation convention with repeated index i ranging from 1 to 3 is implied.

2.2. Strain field

The description of the strain field is directly derived from the 3D continuum theory in accordance with the GEBT framework. The Green-Lagrange (GL) tensor $\mathbf{E}$ is chosen as a strain measure since it includes second-order terms in the generalized strains which may be relevant for fast rotating blades, as shown later. It is written as

$$\mathbf{E} = \frac{1}{2}\left(\mathbf{F}^T\mathbf{F} - \mathbf{I}\right) \tag{11}$$

where the deformation gradient tensor $\mathbf{F}$ is expressed in terms of the natural basis vectors as follows [10]

$$\mathbf{F} = \mathbf{g}_i \otimes \mathbf{G}^i \tag{12}$$

The contravariant basis vectors of the reference configuration are given by $\mathbf{G}^i = \frac{1}{2\sqrt{G}} e_{ijk} \mathbf{G}_j \times \mathbf{G}_k = \mathbf{b}_i$, since it is a Cartesian frame, whereas the covariant basis vectors $\mathbf{g}_i$ of the deformed configuration are computed as follows

$$\begin{aligned}
\mathbf{g}_1 &= \frac{\partial \mathbf{x}}{\partial x} = \mathbf{b}_1 + (R+x)\frac{\partial \mathbf{b}_1}{\partial x} + \frac{\partial \mathbf{u}}{\partial x} + \frac{\partial \mathbf{R}}{\partial x} \cdot \mathbf{R}^T \cdot \boldsymbol{\xi} = \mathbf{b}_1 + \frac{\partial \mathbf{u}}{\partial x} + \mathbf{k} \times \boldsymbol{\xi} = \\
&= (1 + e + zk_2 - yk_3)\,\mathbf{t}_1 + (2\gamma_{12} - zk_1)\,\mathbf{t}_2 + (2\gamma_{13} + yk_1)\,\mathbf{t}_3 \\
\mathbf{g}_2 &= \frac{\partial \mathbf{x}}{\partial y} = \mathbf{R} \cdot \frac{\partial \boldsymbol{\xi}_0}{\partial y} = \mathbf{R} \cdot \mathbf{b}_2 = \mathbf{t}_2 \\
\mathbf{g}_3 &= \frac{\partial \mathbf{x}}{\partial z} = \mathbf{R} \cdot \frac{\partial \boldsymbol{\xi}_0}{\partial z} = \mathbf{R} \cdot \mathbf{b}_3 = \mathbf{t}_3
\end{aligned} \tag{13}$$

In the above expressions, the axial stretch e introduced before is given by $\mathbf{t}_1 \cdot \mathbf{g}_{1(y,z=0)} - 1$, while the shear strains $2\gamma_{1\alpha} = \mathbf{t}_\alpha \cdot \mathbf{g}_{1(y,z=0)}$ $(\alpha = 2, 3)$ and the deformed twisting curvature k_1 and bending curvatures k_2 and k_3 are defined in the following:

$$\begin{aligned}
2\gamma_{1\alpha} &= R_{\alpha 1} + R_{\alpha 1}\frac{\partial u}{\partial x} + R_{\alpha 2}\frac{\partial v}{\partial x} + R_{\alpha 3}\frac{\partial w}{\partial x} = 0 \\
k_1 &= \frac{\partial R_{2i}}{\partial x} R_{3i} = \frac{\partial \phi}{\partial x} + \frac{1}{(1+e)\,(1+R_{11})}\left(R_{13}\frac{\partial^2 v}{\partial x^2} - R_{12}\frac{\partial^2 w}{\partial x^2}\right) \\
k_2 &= -\frac{\partial R_{1i}}{\partial x} R_{3i} = -\frac{1}{1+e}\left(R_{31}\frac{\partial^2 u}{\partial x^2} + R_{32}\frac{\partial^2 v}{\partial x^2} + R_{33}\frac{\partial^2 w}{\partial x^2}\right) \\
k_3 &= \frac{\partial R_{1i}}{\partial x} R_{2i} = \frac{1}{1+e}\left(R_{21}\frac{\partial^2 u}{\partial x^2} + R_{22}\frac{\partial^2 v}{\partial x^2} + R_{23}\frac{\partial^2 w}{\partial x^2}\right)
\end{aligned} \tag{14}$$

As expected, the null shear contribution ($\gamma_{1\alpha} = 0$) is automatically satisfied by the assumed kinematics. As a result, the deformation gradient $\mathbf{F}$ can be conveniently expressed as

$$\mathbf{F} = (1 + e + zk_2 - yk_3)\,\mathbf{t}_1 \otimes \mathbf{b}_1 - zk_1 \mathbf{t}_2 \otimes \mathbf{b}_1 + yk_1 \mathbf{t}_3 \otimes \mathbf{b}_1 + \mathbf{t}_2 \otimes \mathbf{b}_2 + \mathbf{t}_3 \otimes \mathbf{b}_3 \tag{15}$$

whose components in the mixed basis T/B include only the generalized strain measures. Finally, the GL strain tensor is naturally resolved along the undeformed basis vectors $(\mathbf{b}_i \cdot \mathbf{E} \cdot \mathbf{b}_j)$ to yield

$$\begin{aligned}
&E_{11} = e + zk_2 - yk_3 + \frac{1}{2}\left(e^2 + z^2k_2^2 + y^2k_3^2\right) + zek_2 - yek_3 - zyk_2k_3 + \frac{1}{2}\left(z^2 + y^2\right)k_1^2 \\
&2E_{12} = 2E_{21} = -zk_1 \\
&2E_{13} = 2E_{31} = yk_1 \\
&E_{22},\, E_{33},\, E_{23},\, E_{32} = 0
\end{aligned} \tag{16}$$

From Eq. (16) it is clear that the GL strains contain first- and second-order terms. It is remarkable that the above strains have the same mathematical form as those obtained within the framework of classical beam theory in terms of linearized quantities. However, the first-order (generalized) terms in Eq. (16) are pure strain measures and thus are suitable for a large-displacement small-strain analysis. The aim of the present work is to show that, when rotating beams are considered, the second-order components can be neglected *a-priori* only under certain conditions.

2.3. Principle of virtual work

The principle of virtual work (PVW) will be employed to derive the equations of motion of the rotating beam according to the model described above. The PVW can be written in the following form

$$\delta W_i = \delta W_e \quad \forall \delta \mathbf{x} \quad k.a. \tag{17}$$

where δW_i and δW_e are the internal and external virtual work, respectively.

The internal virtual work is expressed in terms of the GL strains E_{ij} in Eq. (16) and their work-conjugate stresses S_{ij} as follows

$$\delta W_i = \int_V \left(\delta E_{11} S_{11} + 2\delta E_{12} S_{12} + 2\delta E_{13} S_{13}\right) \mathrm{d}V \tag{18}$$

After substituting Eq. (16), the following expression in terms of generalized strain measures is obtained

$$\begin{aligned} \delta W_i = &\int_0^\ell \delta e \int_A S_{11}\left(1 + e + zk_2 - yk_3\right) \mathrm{d}A\mathrm{d}x + \int_0^\ell \delta k_2 \int_A z S_{11}\left(1 + e + zk_2 - yk_3\right) \mathrm{d}A\mathrm{d}x \\ &+ \int_0^\ell \delta k_3 \int_A -y S_{11}\left(1 + e + yk_3 + zk_2\right) \mathrm{d}A\mathrm{d}x + \int_0^\ell \delta k_1 \int_A \left[y S_{13} - z S_{12} + S_{11}\left(z^2 + y^2\right) k_1\right] \mathrm{d}A\mathrm{d}x \end{aligned} \tag{19}$$

which can be compactly written by introducing the generalized axial force F_1 and moments M_1, M_2, M_3 as follows

$$\delta W_i = \int_0^\ell \delta e F_1 \mathrm{d}x + \int_0^\ell \delta k_1 M_1 \mathrm{d}x + \int_0^\ell \delta k_2 M_2 \mathrm{d}x + \int_0^\ell \delta k_3 M_3 \mathrm{d}x \tag{20}$$

It is noted that the generalized forces and moments depend on the deformation itself.

Since free vibrations are studied in this work, the external virtual work includes only the inertial terms and reads

$$\delta W_e = -\int_V \left[\delta \mathbf{u} \cdot \rho \mathbf{a} + (\boldsymbol{\delta\theta} \times \boldsymbol{\xi}) \cdot \rho \mathbf{a}\right] \mathrm{d}V \tag{21}$$

After introducing Eqs. (4) and (5) in the above equation, it takes the explicit form

$$\begin{aligned} \delta W_e = &-\int_0^\ell \left[\delta u m \frac{\partial^2 u}{\partial t^2} + \delta v m \frac{\partial^2 v}{\partial t^2} + \delta w m \frac{\partial^2 w}{\partial t^2}\right] \mathrm{d}x - \int_0^\ell \left[\delta\theta_1 I_1 \frac{\partial \omega_1}{\partial t} + \delta\theta_2 I_2 \frac{\partial \omega_2}{\partial t} + \delta\theta_3 I_3 \frac{\partial \omega_3}{\partial t}\right] \mathrm{d}x \\ &+ \int_0^\ell \left[\delta\theta_1 \left(I_2 - I_3\right) \omega_2 \omega_3 + \delta\theta_2 \left(I_3 - I_1\right) \omega_3 \omega_1 + \delta\theta_3 \left(I_1 - I_2\right) \omega_1 \omega_2\right] \mathrm{d}x \\ &- \Omega^2 \left[\int_0^\ell \delta u m \left(R + x + u\right) \mathrm{d}x + \int_0^\ell \delta v m v \, \mathrm{d}x\right] - 2\Omega \left[\int_0^\ell \delta v m \frac{\partial u}{\partial t} \mathrm{d}x - \int_0^\ell \delta u m \frac{\partial v}{\partial t} \mathrm{d}x\right] \\ &- \Omega^2 \left[\int_0^\ell \delta\theta_1 (I_3 - I_2) R_{33} R_{23} \, \mathrm{d}x + \int_0^\ell \delta\theta_2 (I_2 R_{13} R_{33}) \, \mathrm{d}x - \int_0^\ell \delta\theta_3 (I_3 R_{13} R_{23}) \, \mathrm{d}x\right] \\ &- 2\Omega \left[\int_0^\ell \delta\theta_1 \left(I_3 R_{23} \omega_3 - I_2 R_{33} \omega_2\right) \mathrm{d}x + \int_0^\ell \delta\theta_2 \left(I_2 R_{33}\right) \omega_1 \, \mathrm{d}x - \int_0^\ell \delta\theta_3 \left(I_3 R_{23}\right) \omega_1 \, \mathrm{d}x\right] \end{aligned} \tag{22}$$

where $m = \rho A$ is the mass per unit length of the beam, I_3 and I_2 are the cross-sectional mass moments of inertia with respect to y and z axis, respectively, and $I_1 = I_2 + I_3$ is the mass polar moment of inertia of the cross section.

3. Equilibrium configuration

This study is focused on small perturbations about the equilibrium configuration of the rotating beam. As explained in the next section, a linearization process is directly carried out in the PVW equation. This simplifies a lot the mathematical derivation, once the equilibrium condition is appropriately determined. In the case of planar rotating beams, the equilibrium state is the solution of a linear problem under the assumption of small strains, as shown below. This is not valid in general, as in the case of a tilted beam, for which the determination of the equilibrium condition is a nonlinear problem even in the case of small strains. However, it is believed that the novelty of the present work is not limited since the effect of the fully consistent linearization process outlined in the following can be pointed out anyway. Actually, the simplicity of the problem allows to clearly highlight the additional stiffening terms in the linearized equations of motion when second-order generalized strains are retained.

For the problem under investigation, the equilibrium configuration of the rotating beam is characterized by an axial deformation $\bar{u}$ only, due to the centrifugal acceleration arising from the constant angular velocity. Therefore, the equilibrium state is identified by

$$u = \bar{u} \quad \bar{v},\, \bar{w},\, \bar{\phi} = 0 \tag{23}$$

Accordingly, the motion of the beam can be expressed as

$$u = \bar{u} + \Delta u \qquad v = \Delta v \qquad w = \Delta w \qquad \phi = \Delta\phi \tag{24}$$

where Δ terms represent the perturbations about the equilibrium condition.

If the axial strain is assumed to be sufficiently small, i.e., $\bar{e} = \partial\bar{u}/\partial x \ll 1$, a *physically linear* constitutive law can be employed to yield the following equilibrium equation expressed in weak form:

$$\int_0^\ell \frac{\partial\delta\Delta u}{\partial x} EA \frac{\partial\bar{u}}{\partial x}\mathrm{d}x = -\Omega^2 \int_0^\ell \delta\Delta u\, m\,(R + x + \bar{u})\,\mathrm{d}x \tag{25}$$

After integrating by parts the left-hand side in Eq. (25), imposing null displacement at $x = 0$ and exploiting the arbitrariness of the virtual variation at the free end, the following boundary-value problem is obtained:

$$\begin{cases} EA\dfrac{\partial^2\bar{u}^{(\mathrm{L})}}{\partial x^2} + \rho\Omega^2\bar{u}^{(\mathrm{L})} + \rho\Omega^2\,(R + x) = 0 \\ \bar{u}^{(\mathrm{L})}(0) = 0 \qquad \dfrac{\partial\bar{u}^{(\mathrm{L})}}{\partial x}(\ell) = 0 \end{cases} \tag{26}$$

where the notation $\bar{u}^{(\mathrm{L})}$ is adopted for the small but finite axial displacement of the beam corresponding to the linearized equilibrium configuration given by Eq. (25). The solution can be expressed in terms of the nondimensional extension $\hat{\bar{u}} = \bar{u}/\ell$ as follows

$$\hat{\bar{u}}^{(\mathrm{L})}(\xi) = \frac{\hat{\Omega}\,\delta\cos\left[\hat{\Omega}\,(1-\xi)\right] + \sin(\hat{\Omega}\xi)}{\hat{\Omega}\cos(\hat{\Omega})} - \delta + \xi \tag{27}$$

where $\xi = x/\ell$ is the dimensionless axial coordinate, $\hat{\Omega} = \Omega\sqrt{\rho\ell^2/E}$ is the dimensionless angular velocity, and $\delta = R/\ell$ is the hub radius ratio. It is clear that the above linear model is divergent when $\hat{\Omega} = \pi/2$, which corresponds to an angular velocity equal to the first axial frequency of a non-rotating beam.

What presented so far assumes strain values sufficiently small so that the equilibrium condition falls within the linear elastic range. Since the strain of the rotating beam is related to its angular speed, there is the need of evaluating the range of validity of the equilibrium configuration in Eq. (27) in terms of angular velocity, i.e., the maximum value of the angular speed for which the constitutive law is linear in the strains. For this purpose, the above linear solution is compared with a nonlinear solution obtained from the following equilibrium condition as proposed by Hodges and Bless [8]:

$$\int_0^\ell \frac{\partial \delta\Delta u}{\partial x} EA \left[\frac{\partial \bar{u}}{\partial x} + \beta\left(\frac{\partial \bar{u}}{\partial x}\right)^2\right] \mathrm{d}x = -\Omega^2 \int_0^\ell \delta\Delta u\, m\,(R + x + \bar{u})\,\mathrm{d}x \tag{28}$$

where $\beta \approx O(1)$ is a dimensionless constant which depends upon the material and section geometry of the beam and must be determined experimentally. What expressed in Eq. (28) relies on a *physically nonlinear* 1-D constitutive law ($\beta \neq 0$) and can be viewed as an exact analysis valid for large strains, where the term exact is here adopted to refer to the computation of the equilibrium axial displacement without any additional approximation compared to the simplifying assumptions already introduced. When $R = 0$, an approximated solution of Eq. (28) is given by [8]

$$\hat{\bar{u}}^{(\mathrm{NL})}(\xi) = \left[\frac{\sqrt{1764 - 1428\,\hat{\Omega}^2 + 3024\,\beta\,\hat{\Omega}^2 + 289\,\hat{\Omega}^4} - 42 + 17\,\hat{\Omega}^2}{36\,\beta}\right]\left(\frac{\xi}{2} - \frac{\xi^3}{6}\right) \tag{29}$$

It can be shown that the solution in Eq. (29) is accurate when $\hat{\Omega} < \pi^2/4$ and the corresponding model shows no divergence instability for stiffening-like materials ($\beta > 0$).

With the aim of comparing the equilibrium state computed from the physically linear and nonlinear constitutive law, the tip displacement $\hat{\bar{u}}(1)$ evaluated for both cases when $\delta = 0$ is shown in Figure 3 as a function of the nondimensional rotating speed $\hat{\Omega}$. The values corresponding to the nonlinear approach are computed by assuming $\beta = 0.5$. Similarly, the corresponding root strain $\bar{e}_{root}$ for the two cases is reported in Figure 4. Since the maximum axial strain occurs at the root for rotating cantilever uniform beams, $\bar{e}_{root}$ can be taken as a measure of the overall deformation level of the beam. It is observed that the displacement and strain curves computed using the linear and nonlinear formulation begin to differ from each other at a value of the dimensionless angular velocity $\hat{\Omega}$ of about 0.3. The physically nonlinear and linear solutions give extremely close results if the dimensionless angular speed is less than 0.2, which corresponds to a root axial strain of approximately 2% (see Figure 4).

When $\bar{e} \ll 1$, the axial strain at the root of the beam can be approximated as follows

$$\bar{e}_{root} = \hat{\Omega}^2\left(\delta + \frac{1}{2}\right) \tag{30}$$

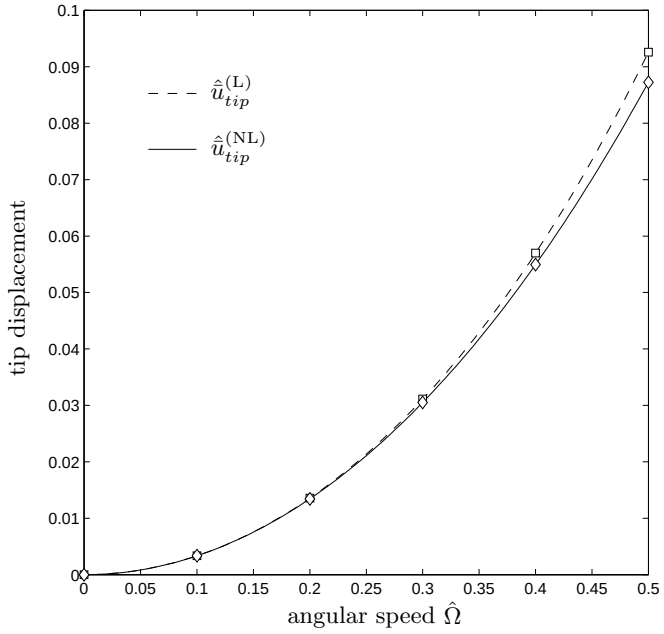

Figure 3: Axial tip displacement in the equilibrium configuration as a function of the dimensionless angular velocity $\hat{\Omega}$.

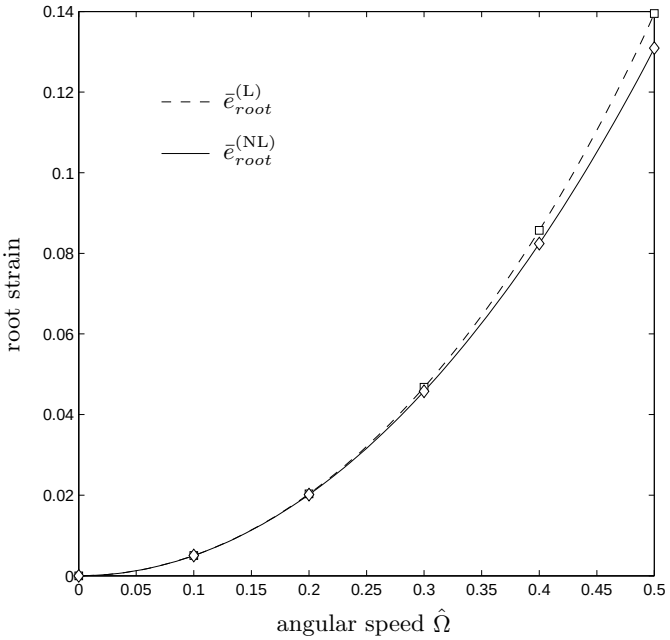

Figure 4: Axial root strain in the equilibrium configuration as a function of the dimensionless angular velocity $\hat{\Omega}$.

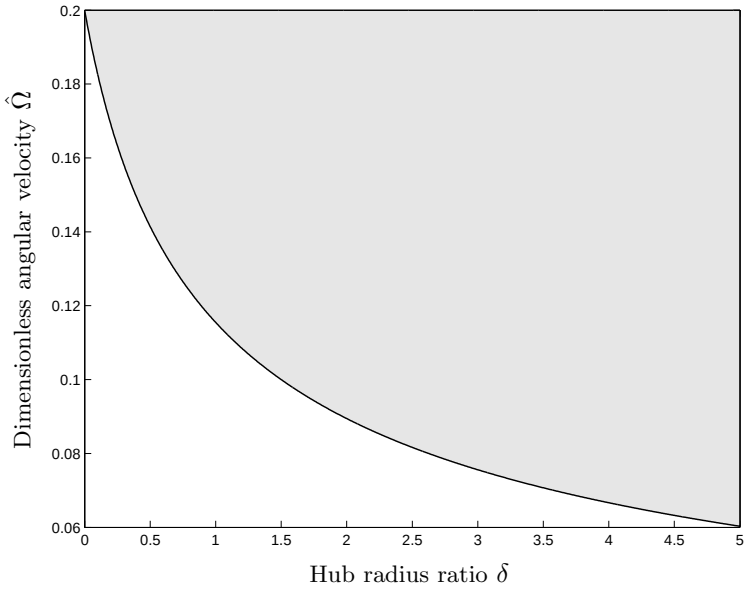

Figure 5: Variation of the maximum dimensionless angular velocity $\hat{\Omega}_{\max}$ with the hub radius ratio δ for a maximum root strain of 2%.

Solving for the dimensionless angular velocity and setting a maximum root strain of 2% as observed before yields

$$\hat{\Omega}_{\max} = \sqrt{\frac{0.02}{\delta + 0.5}} \tag{31}$$

which can be used to compute the limit value of the angular speed of a rotating beam with hub radius ratio δ for which the equilibrium configuration is subject to sufficiently small strain so that a physically linear constitutive law applies. For the sake of convenience, Eq. (31) is graphically represented in Figure 5, where the shadowed region denotes values of $\hat{\Omega}$ beyond the validity range of the model. The decreasing trend of the maximum angular velocity with increasing values of the hub radius ratio δ can be also explained from physical reasoning. Indeed, the axial stress arising from the centrifugal acceleration increases with the distance R from the centre of rotation and, consequently, it induces larger axial strains at the root of the beam for higher values of δ. In the following, high angular speeds will denote equilibrium conditions falling inside the non-shadowed region in Figure 5 close to the dividing line. As a final remark, it is observed that the instability predicted by the model based on the physically linear constitutive law occurs at an angular velocity $\hat{\Omega} = \pi/2$ which is largely beyond the range where the strains can be correctly assumed to be small. Therefore, the instability condition related to the equilibrium configuration of the linear model is actually meaningless.

4. Fully consistent linearization of the principle of virtual work

4.1. Incremental analysis

As already outlined, the linearization procedure is performed directly in the PVW. According to the Total Lagrangian approach, the axial stretch and curvatures are written as

$$e = \bar{e} + \Delta e \qquad k_i = \Delta k_i \qquad (i = 1, 2, 3) \tag{32}$$

where $\bar{e}$ is referred to the equilibrium condition $(\bar{u}, 0, 0, 0)$ and Δ terms are incremental quantities. The twisting and bending curvatures are set equal to the increments since their values are zero in the equilibrium configuration (see Eq. (23)). Inserting Eq. (32) into Eq. (16) yields

$$E_{11} = \bar{E}_{11} + \Delta E_{11} \qquad 2E_{12} = 2\Delta E_{12} \qquad 2E_{13} = 2\Delta E_{13} \tag{33}$$

where $\bar{E}_{11} = \bar{e} + (1/2)\bar{e}^2$ is the value at the equilibrium state and

$$\begin{aligned} \Delta E_{11} &= \bar{\nu}\left(\Delta e + z\Delta k_2 - y\Delta k_3\right) + z\Delta e\Delta k_2 - y\Delta e\Delta k_3 - zy\Delta k_2\Delta k_3 \\ &\quad + \frac{1}{2}\left[\Delta e^2 + z^2\Delta k_2^2 + y^2\Delta k_3^2 + \left(z^2 + y^2\right)\Delta k_1^2\right] \\ 2\Delta E_{12} &= -z\Delta k_1 \\ 2\Delta E_{13} &= y\Delta k_1 \end{aligned} \tag{34}$$

with $\bar{\nu} = 1 + \bar{e}$. It is noted that quadratic terms are retained in the expression of ΔE_{11}. This is crucial in performing a fully consistent linearization without missing any contribution in the linearized equations of motion, as shown in the following.

Since $\bar{E}_{11}$ is prescribed, i.e., $\delta\bar{E}_{11} = 0$, the internal virtual work takes the form

$$\delta W_i = \int_V \left[\delta\Delta E_{11}\left(\bar{\sigma}_{11} + \Delta S_{11}\right) + 2\delta\Delta E_{12}\Delta S_{12} + 2\delta\Delta E_{13}\Delta S_{13}\right] \mathrm{d}V \tag{35}$$

where $\bar{\sigma}_{11}$ is the axial stress corresponding to the equilibrium configuration and acting as a pre-stress condition for the actual deformation of the beam, and ΔS_{11}, ΔS_{12} and ΔS_{13} are the components of the incremental stress tensor. According to Eq. (34), the virtual variations of the incremental strains are given by

$$\begin{aligned} \delta\Delta E_{11} &= \bar{\nu}\left(\delta\Delta e + z\delta\Delta k_2 - y\delta\Delta k_3\right) + z\delta(\Delta e\Delta k_2) - y\delta(\Delta e\Delta k_3) - zy\delta(\Delta k_2\Delta k_3) \\ &\quad + \delta\Delta e\Delta e + z^2\delta\Delta k_2\Delta k_2 + y^2\delta\Delta k_3\Delta k_3 + (z^2 + y^2)\delta\Delta k_1\Delta k_1 \\ 2\delta\Delta E_{12} &= -z\delta\Delta k_1 \\ 2\delta\Delta E_{13} &= y\delta\Delta k_1 \end{aligned} \tag{36}$$

In the framework of a linear elastic constitutive law for isotropic materials, it follows that the incremental stress and strain quantities are related by

$$\left\{ \begin{array}{c} \Delta S_{11} \\ \Delta S_{12} \\ \Delta S_{13} \end{array} \right\} = \left[\begin{array}{ccc} E & 0 & 0 \\ 0 & G & 0 \\ 0 & 0 & G \end{array} \right] \left\{ \begin{array}{c} \Delta E_{11} \\ 2\Delta E_{12} \\ 2\Delta E_{13} \end{array} \right\} \tag{37}$$

where G is the shear modulus.

4.2. Internal virtual work

After substituting Eqs. (36) and (37) into Eq. (35), and discarding higher-order terms, including those which contain $\bar{e}^2$ according to what shown in the previous section, the internal virtual work can be approximated as the summation of two contributions as follows

$$\delta W_i \approx \delta W_i^{(\mathrm{L})} + \delta W_i^{(\mathrm{G})} \tag{38}$$

The first term is responsible for the classical linear elastic stiffness of the flexible beam. It is expressed as

$$\delta W_i^{(\mathrm{L})} = \int_0^\ell \left[\delta\Delta e \, EA\Delta e + \delta\Delta k_2 \, EJ_2\Delta k_2 + \delta\Delta k_3 \, EJ_3\Delta k_3 + \delta\Delta k_1 \, GJ\Delta k_1 \right] \mathrm{d}x \tag{39}$$

where J_2 and J_3 are the cross-sectional area moments of inertia with respect to z and y axis, respectively, and GJ is the torsional stiffness. The quantity $\delta W_i^{(\mathrm{G})}$ refers to the geometric stiffening induced by the pre-stress $\bar{\sigma}_{11}$. For the sake of convenience, it is divided into two separate contributions as follows

$$\delta W_i^{(\mathrm{G})} = \delta W_i^{(\mathrm{G}_1)} + \delta W_i^{(\mathrm{G}_2)} \tag{40}$$

where

$$\delta W_i^{(\mathrm{G}_1)} = \int_0^\ell \left[\delta\Delta e \, \bar{\sigma}_{11} A \left(\bar{\nu} + \Delta e \right) + \delta\Delta k_2 \, \bar{\sigma}_{11} J_2 \Delta k_2 + \delta\Delta k_3 \, \bar{\sigma}_{11} J_3 \Delta k_3 + \delta\Delta k_1 \, \bar{\sigma}_{11} J_1 \Delta k_1 \right] \mathrm{d}x \tag{41}$$

$$\delta W_i^{(\mathrm{G}_2)} = 2 \int_0^\ell \left[\delta\Delta e \, EA \, \bar{e}\Delta e + \delta\Delta k_2 \, EJ_2 \, \bar{e}\Delta k_2 + \delta\Delta k_3 \, EJ_3 \, \bar{e}\Delta k_3 \right] \mathrm{d}x \tag{42}$$

and $J_1 = J_2 + J_3$. The second contribution $\delta W_i^{(\mathrm{G}_2)}$ includes the stiffening accounting for the pre-deformation of the beam related to the equilibrium configuration. It is worth noting that, in the above expressions, all quantities are referred to the principal centroidal axes of the cross-section, i.e., $\int_A y \mathrm{d}A = \int_A z \mathrm{d}A = \int_A yz \mathrm{d}A = 0$.

With the aim of writing the internal virtual work as a function of displacement variables, the incremental values Δe, Δk_i must be expressed in terms of Δu, Δv, Δw and $\Delta\phi$. However, referring to Eqs. (8) and (14), it is clear that the axial stretch and curvatures are nonlinear functions of the displacements and twist angle. The same applies for the increments. Since a fully consistent linearized model can be obtained from

quadratic terms in Eqs. (39), (41) and (42), an appropriate truncated expansion of each generalized strain should be devised. Due to the presence of $\int_0^\ell \delta\Delta e\,(\bar{\sigma}_{11}A\bar{\nu})\,\mathrm{d}x$ in the geometric contribution $\delta W_i^{(\mathrm{G}_1)}$, which contains the zeroth-order term $\bar{\sigma}_{11}$, the axial stretch is expanded up to the second order. In so doing, the corresponding virtual variation contains all the quantities which can contribute to the resulting linearized model. It follows that the increment Δe is given by

$$\Delta e = \frac{\partial \Delta u}{\partial x} + \frac{1}{2}\frac{1}{\bar{\nu}}\left(\frac{\partial \Delta v}{\partial x}\right)^2 + \frac{1}{2}\frac{1}{\bar{\nu}}\left(\frac{\partial \Delta w}{\partial x}\right)^2 \tag{43}$$

Accordingly, the virtual variation is written as

$$\delta\Delta e = \frac{\partial \delta\Delta u}{\partial x} + \frac{1}{\bar{\nu}}\frac{\partial \Delta v}{\partial x}\frac{\partial \delta\Delta v}{\partial x} + \frac{1}{\bar{\nu}}\frac{\partial \Delta w}{\partial x}\frac{\partial \delta\Delta w}{\partial x} \tag{44}$$

Instead, the curvatures are expanded to the first-order to yield

$$\Delta k_1 = \frac{\partial \Delta\phi}{\partial x} \qquad \Delta k_2 = -\frac{1}{\bar{\nu}}\frac{\partial^2 \Delta w}{\partial x^2} \qquad \Delta k_3 = \frac{1}{\bar{\nu}}\frac{\partial^2 \Delta v}{\partial x^2} \tag{45}$$

Substituting Eqs. (43), (44) and (45) into the above linear and geometric contributions, and neglecting higher-order terms, the linearized internal virtual work is finally expressed as

$$\begin{aligned}\delta W_i = \overline{\delta W_i} + \int_0^\ell \Bigg[& \frac{\partial \delta\Delta u}{\partial x} EA \frac{\partial \Delta u}{\partial x} + \frac{\partial^2 \delta\Delta v}{\partial x^2}\frac{EJ_3}{\bar{\nu}^2}\frac{\partial^2 \Delta v}{\partial x^2} + \frac{\partial^2 \delta\Delta w}{\partial x^2}\frac{EJ_2}{\bar{\nu}^2}\frac{\partial^2 \Delta w}{\partial x^2} + \frac{\partial \delta\Delta\phi}{\partial x} GJ \frac{\partial \Delta\phi}{\partial x} \\ & + 3\left(\frac{\partial \delta\Delta u}{\partial x}\bar{\sigma}_{11}A\frac{\partial \Delta u}{\partial x} + \frac{\partial^2 \delta\Delta v}{\partial x^2}\frac{\bar{\sigma}_{11}J_3}{\bar{\nu}^2}\frac{\partial^2 \Delta v}{\partial x^2} + \frac{\partial^2 \delta\Delta w}{\partial x^2}\frac{\bar{\sigma}_{11}J_2}{\bar{\nu}^2}\frac{\partial^2 \Delta w}{\partial x^2}\right) \\ & + \frac{\partial \delta\Delta v}{\partial x}\bar{\sigma}_{11}A\frac{\partial \Delta v}{\partial x} + \frac{\partial \delta\Delta w}{\partial x}\bar{\sigma}_{11}A\frac{\partial \Delta w}{\partial x} + \frac{\partial \delta\Delta\phi}{\partial x}\bar{\sigma}_{11}J_1\frac{\partial \Delta\phi}{\partial x}\Bigg]\,\mathrm{d}x\end{aligned} \tag{46}$$

where

$$\overline{\delta W_i} = \int_0^\ell \frac{\partial \delta\Delta u}{\partial x} EA \frac{\partial \bar{u}}{\partial x}\mathrm{d}x \tag{47}$$

4.3. External virtual work

The linearization of Eq. (22) yields the following expression for the inertial virtual work of the rotating beam

$$\begin{aligned}\delta W_e = \overline{\delta W_e} - \int_0^\ell \Bigg\{ & \delta\Delta u\left(m\frac{\partial^2 \Delta u}{\partial t^2} - 2m\Omega\frac{\partial \Delta v}{\partial t} - m\Omega^2\Delta u\right) + \delta\Delta v\left(m\frac{\partial^2 \Delta v}{\partial t^2} + 2m\Omega\frac{\partial \Delta u}{\partial t} - m\Omega^2\Delta v\right) \\ & + \delta\Delta w\, m\frac{\partial^2 \Delta w}{\partial t^2} + \delta\Delta\phi\left[I_1\frac{\partial^2 \Delta\phi}{\partial t^2} - \Omega^2\left(I_2 - I_3\right)\Delta\phi + 2\Omega\frac{I_2}{\bar{\nu}}\frac{\partial^2 \Delta w}{\partial t \partial x}\right] \\ & + \frac{\partial \delta\Delta v}{\partial x}\frac{I_3}{\bar{\nu}^2}\frac{\partial^3 \Delta v}{\partial t^2 \partial x} + \frac{\partial \delta\Delta w}{\partial x}\left(\frac{I_2}{\bar{\nu}^2}\frac{\partial^3 \Delta w}{\partial t^2 \partial x} - 2\Omega\frac{I_2}{\bar{\nu}}\frac{\partial \Delta\phi}{\partial t} - \frac{I_2}{\bar{\nu}^2}\Omega^2\frac{\partial \Delta w}{\partial x}\right)\Bigg\}\,\mathrm{d}x\end{aligned} \tag{48}$$

where

$$\overline{\delta W_e} = -\Omega^2\left[\int_0^\ell \delta\Delta u\, m\left(R + x + \bar{u}\right)\right]\mathrm{d}x \tag{49}$$

Note that the equilibrium configuration is given by $\overline{\delta W_i} = \overline{\delta W_e}$.

5. Equations of motion

The set of linear equations of motion of the rotating beam can be obtained from the linearized expressions in Eqs. (46) and (48). After integrating by parts those terms in the internal and inertial virtual work involving derivatives of the virtual quantities and exploiting the arbitrariness of the virtual variations in the beam domain, the equations for the axial, chordwise, flapwise and torsional vibrations, respectively, are written as

$$EA\frac{\partial^2\Delta u}{\partial x^2}+3A\frac{\partial}{\partial x}\left(\bar{\sigma}_{11}\frac{\partial\Delta u}{\partial x}\right)=m\frac{\partial^2\Delta u}{\partial t^2}-2m\Omega\frac{\partial\Delta v}{\partial t}-m\Omega^2\Delta u \tag{50}$$

$$\begin{aligned}&EJ_3\frac{\partial^2}{\partial x^2}\left(\frac{1}{\bar{\nu}^2}\frac{\partial^2\Delta v}{\partial x^2}\right)+3J_3\frac{\partial^2}{\partial x^2}\left(\frac{\bar{\sigma}_{11}}{\bar{\nu}^2}\frac{\partial^2\Delta v}{\partial x^2}\right)-\frac{\partial}{\partial x}\left(\bar{N}\frac{\partial\Delta v}{\partial x}\right)\\&\quad+m\frac{\partial^2\Delta v}{\partial t^2}+2m\Omega\frac{\partial\Delta u}{\partial t}-m\Omega^2\Delta v-I_3\frac{\partial}{\partial x}\left(\frac{1}{\bar{\nu}^2}\frac{\partial^3\Delta v}{\partial x\partial t^2}\right)=0\end{aligned} \tag{51}$$

$$\begin{aligned}&EJ_2\frac{\partial^2}{\partial x^2}\left(\frac{1}{\bar{\nu}^2}\frac{\partial^2\Delta w}{\partial x^2}\right)+3J_2\frac{\partial^2}{\partial x^2}\left(\frac{\bar{\sigma}_{11}}{\bar{\nu}^2}\frac{\partial^2\Delta w}{\partial x^2}\right)-\frac{\partial}{\partial x}\left(\bar{N}\frac{\partial\Delta w}{\partial x}\right)\\&\quad+m\frac{\partial^2\Delta w}{\partial t^2}+2I_2\Omega\frac{\partial}{\partial x}\left(\frac{1}{\bar{\nu}}\frac{\partial\Delta\phi}{\partial t}\right)+I_2\Omega^2\frac{\partial}{\partial x}\left(\frac{1}{\bar{\nu}^2}\frac{\partial\Delta w}{\partial x}\right)-I_2\frac{\partial}{\partial x}\left(\frac{1}{\bar{\nu}^2}\frac{\partial^3\Delta w}{\partial x\partial t^2}\right)=0\end{aligned} \tag{52}$$

$$GJ\frac{\partial^2\Delta\phi}{\partial x^2}+J_1\frac{\partial}{\partial x}\left(\bar{\sigma}_{11}\frac{\partial\Delta\phi}{\partial x}\right)=I_1\frac{\partial^2\Delta\phi}{\partial t^2}+2\frac{I_2}{\bar{\nu}}\Omega\frac{\partial^2\Delta w}{\partial t\partial x}-\left(I_2-I_3\right)\Omega^2\Delta\phi \tag{53}$$

where $\bar{N}=\bar{\sigma}_{11}A$.

The set of partial differential equations shown above is associated with the following boundary conditions for the cantilever case:

$$x=0:\begin{cases}\Delta u=0\\ \dfrac{\partial\Delta v}{\partial x}=0\\ \Delta v=0\\ \dfrac{\partial\Delta w}{\partial x}=0\\ \Delta w=0\\ \Delta\phi=0\end{cases}\qquad x=\ell:\begin{cases}EA\dfrac{\partial\Delta u}{\partial x}=0\\ \dfrac{EJ_3}{\bar{\nu}^2}\dfrac{\partial^2\Delta v}{\partial x^2}=0\\ \dfrac{I_3}{\bar{\nu}^2}\dfrac{\partial^3\Delta v}{\partial t^2\partial x}-EJ_3\dfrac{\partial}{\partial x}\left(\dfrac{1}{\bar{\nu}^2}\dfrac{\partial^2\Delta v}{\partial x^2}\right)=0\\ \dfrac{EJ_2}{\bar{\nu}^2}\dfrac{\partial^2\Delta w}{\partial x^2}=0\\ \dfrac{I_2}{\bar{\nu}^2}\dfrac{\partial^3\Delta w}{\partial t^2\partial x}-2\dfrac{I_2}{\bar{\nu}}\Omega\dfrac{\partial\Delta\phi}{\partial t}-\dfrac{I_2}{\bar{\nu}^2}\Omega^2\dfrac{\partial\Delta w}{\partial x}-EJ_2\dfrac{\partial}{\partial x}\left(\dfrac{1}{\bar{\nu}^2}\dfrac{\partial^2\Delta w}{\partial x^2}\right)=0\\ GJ\dfrac{\partial\Delta\phi}{\partial x}=0\end{cases} \tag{54}$$

Some general observations are worth noting about the linearized equations obtained before.

First of all, the four equations are coupled two by two, so the two sets can be studied separately, as already shown by Lacarbonara et al. [17]. The axial and chordwise equations of motion (Eq. (50) and (51),

respectively) are coupled with each other through the classical gyroscopic terms $2m\Omega\frac{\partial\Delta v}{\partial t}$ and $2m\Omega\frac{\partial\Delta v}{\partial t}$, as expected. The same applies for flapwise and torsional vibrations (Eq. (52) and (53)). However, here the gyroscopic coupling arises from terms containing the rotary inertia I_2, whose contribution to the inertial work is neglected in many formulations. When the flapwise/torsional coupling is omitted, the accuracy of results could decrease for large values of the angular velocity, where the value of $I_2\Omega$ becomes relevant. In the light of this, it also follows that both coupling effects can be reasonably ignored when the angular speed is very small. In this case the axial, torsional, x-y and x-z bending natural frequencies can be accurately computed by solving the related single equations.

It is also noted that some additional terms appear in the flapwise and torsional equations when the rotary inertia of the rotating beam is taken into account. Again, their contribution increases at high angular velocity. In particular, it is observed that the acceleration term $-\left(I_2 - I_3\right)\Omega^2\Delta\phi$ in Eq. (53) for torsion vanishes for doubly-symmetric cross-sections, as expected, differently from the quantity $-I_2\Omega^2\Delta\phi$ which is obtained from classical linearized theories.

It is seen that the centrifugal stiffening terms $\frac{\partial}{\partial x}\left(\bar{N}\frac{\partial\Delta v}{\partial x}\right)$ and $\frac{\partial}{\partial x}\left(\bar{N}\frac{\partial\Delta w}{\partial x}\right)$, which are present in many formulations of rotating beams, are naturally obtained in the chordwise and flapwise equations of motion. However, the fully consistent linearization explained in the previous section leads to some non-classical stiffening terms, which are absent in those approaches that neglect *a-priori* the quadratic components of the generalized strains. This is true for classical methods based on von-Karman nonlinearities, but also for GEBTs based on the Jaumann strain tensor $\mathbf{B}$ under small local rotation and strains. Indeed, a consistent approximation of $\mathbf{B}$ is $B_{ij} = (F_{ij} + F_{ji})/2 - \delta_{ij}$, where $F_{ij} = \mathbf{t}_i \cdot \mathbf{F} \cdot \mathbf{b}_j$ are the components of the deformation gradient in the mixed basis. The components of the approximate Jaumann strain tensor in terms of generalized strains are $B_{11} = e + zk_y - yk_z$, $2B_{12} = -zk_x$, $2B_{13} = yk_x$, and $B_{22} = B_{33} = B_{23} = B_{32} = 0$, which are exactly the Green-Lagrange strains when second-order generalized terms are neglected (see Eq. (16)). Therefore, when the internal virtual work is linearized, only the geometric contribution of $\int_0^\ell \delta\Delta e\bar{\sigma}_{11}A\bar{\nu}\mathrm{d}x$ is captured, which includes the stiffening effect connected to the coupling among axial and transversal displacement, the so-called foreshortening effect.

According to the consistent linearization proposed in this work, the axial equation contains the quantity $3A\frac{\partial}{\partial x}\left(\bar{\sigma}_{11}\frac{\partial\Delta u}{\partial x}\right)$, which expresses the increase of the elastic axial stiffness due to the pre-stress and pre-deformation associated with the equilibrium condition. To the best of the authors' knowledge, this axial stiffening contribution was not previously studied in the open literature and its effect will be investigated in detail in the numerical analysis. Note also that, since the axial motion is coupled with the chordwise motion through the gyroscopic terms, the bending vibrations in the x-y plane are also increasingly affected by the axial stiffening effect as the angular speed increases.

Stiffening terms of the same nature are also present in Eqs. (51), (52) and (53). The quantities

$3J_3\frac{\partial^2}{\partial x^2}\left(\frac{\bar{\sigma}_{11}}{\bar{\nu}^2}\frac{\partial^2\Delta v}{\partial x^2}\right)$ and $3J_2\frac{\partial^2}{\partial x^2}\left(\frac{\bar{\sigma}_{11}}{\bar{\nu}^2}\frac{\partial^2\Delta w}{\partial x^2}\right)$ involve an increased bending stiffness in the two planes. The quantity $J_1\frac{\partial}{\partial x}\left(\bar{\sigma}_{11}\frac{\partial\Delta\phi}{\partial x}\right)$ identifies the increase of the torsional stiffness due to extension-twist coupling of the beam subject to the centrifugal force. This effect is known as trapeze effect, and it is extremely relevant for torsionally soft beams, which is not the case addressed in this study. Further details and discussion on the trapeze effect can be found in the book of Hodges [10] and the references cited therein.

6. Ritz-Galerkin discretization

The equations of motion presented in Section 5 along with the set of boundary conditions corresponding to a cantilever rotating beam are difficult to be solved exactly. For this purpose, many semi-analytical and numerical methods can be adopted (see, e.g., Refs. [34, 32, 7, 11]). Here, an approximate solution for free vibration analysis is sought through the Ritz-Galerkin discretization method as follows

$$\begin{cases} u(x,t) = \sum_{j=1}^{N_\mathrm{u}} \Phi_{\mathrm{u}j}(x) q_{\mathrm{u}j}(t) \\ v(x,t) = \sum_{l=1}^{N_\mathrm{v}} \Phi_{\mathrm{v}l}(x) q_{\mathrm{v}l}(t) \\ w(x,t) = \sum_{n=1}^{N_\mathrm{w}} \Phi_{\mathrm{w}n}(x) q_{\mathrm{w}n}(t) \\ \phi(x,t) = \sum_{s=1}^{N_\phi} \Phi_{\phi s}(x) q_{\phi s}(t) \end{cases} \tag{55}$$

where $\Phi_{\mathrm{u}j}(x)$, $\Phi_{\mathrm{v}l}(x)$, $\Phi_{\mathrm{w}n}(x)$ and $\Phi_{\phi s}(x)$ is the generic term of the complete set of assumed admissible functions for the axial, chordwise and flapwise displacement u, v and w, and for the twist angle ϕ, respectively, and $q_{\mathrm{u}j}(t)$, $q_{\mathrm{v}l}(t)$, $q_{\mathrm{w}n}(t)$ and $q_{\phi s}(t)$ is the related time-dependent generalized coordinate. In Eq. (55), the four variables are expanded as series with N_u, N_v, N_w and N_ϕ number of terms, respectively. Since this study is devoted to the analysis of a cantilever beam, the admissible functions must be selected to satisfy at least the essential boundary conditions at $x = 0$ reported in Eq. (54).

The assumed solution of Eq. (55) is directly substituted into the linearized virtual work quantities in Eqs. (46) and (48) for both displacement quantities and their virtual variations. The discretized equations of motion are then obtained by exploiting the arbitrariness of the virtual variations of the generalized coordinates $\delta q_{\mathrm{u}i}$, $\delta q_{\mathrm{v}k}$, $\delta q_{\mathrm{w}m}$ and $\delta q_{\phi r}$, where $i = 1, \ldots, N_\mathrm{u}$, $k = 1, \ldots, N_\mathrm{v}$, $m = 1, \ldots, N_\mathrm{w}$ and $r = 1, \ldots, N_\phi$.

After some manipulations, they can be expressed in compact indicial form as follows

$$\begin{cases} \displaystyle\sum_{j=1}^{N_{\mathrm{u}}} \left[M_{ij}^{\mathrm{uu}} \frac{\mathrm{d}^2 q_{\mathrm{u}j}}{\mathrm{d}t^2} - G_{il}^{\mathrm{uv}} \frac{\mathrm{d}q_{\mathrm{v}l}}{\mathrm{d}t} + \left(K_{ij}^{\mathrm{uu(L)}} + K_{ij}^{\mathrm{uu(G_1)}} + K_{ij}^{\mathrm{uu(G_2)}} - K_{ij}^{\mathrm{uu}(\Omega)} \right) q_{\mathrm{u}j} \right] = 0 \\ \displaystyle\sum_{l=1}^{N_{\mathrm{v}}} \left[M_{kl}^{\mathrm{vv}} \frac{\mathrm{d}^2 q_{\mathrm{v}l}}{\mathrm{d}t^2} + G_{kj}^{\mathrm{vu}} \frac{\mathrm{d}q_{\mathrm{u}j}}{\mathrm{d}t} + \left(K_{kl}^{\mathrm{vv(L)}} + K_{kl}^{\mathrm{vv(G_1)}} + K_{kl}^{\mathrm{vv(G_2)}} - K_{kl}^{\mathrm{vv}(\Omega)} \right) q_{\mathrm{v}l} \right] = 0 \\ \displaystyle\sum_{n=1}^{N_{\mathrm{w}}} \left[M_{mn}^{\mathrm{ww}} \frac{\mathrm{d}^2 q_{\mathrm{w}n}}{\mathrm{d}t^2} - G_{ms}^{\mathrm{w}\phi} \frac{\mathrm{d}q_{\phi s}}{\mathrm{d}t} + \left(K_{mn}^{\mathrm{ww(L)}} + K_{mn}^{\mathrm{ww(G_1)}} + K_{mn}^{\mathrm{ww(G_2)}} - K_{mn}^{\mathrm{ww}(\Omega)} \right) q_{\mathrm{w}n} \right] = 0 \\ \displaystyle\sum_{s=1}^{N_{\phi}} \left[M_{rs}^{\phi\phi} \frac{\mathrm{d}^2 q_{\phi s}}{\mathrm{d}t^2} + G_{rn}^{\phi\mathrm{w}} \frac{\mathrm{d}q_{\mathrm{w}n}}{\mathrm{d}t} + \left(K_{rs}^{\phi\phi\mathrm{(L)}} + K_{rs}^{\phi\phi\mathrm{(G_1)}} - K_{rs}^{\phi\phi(\Omega)} \right) q_{rs} \right] = 0 \end{cases} \tag{56}$$

where the mass, gyroscopic and stiffness quantities are explicitly given in the Appendix. It is noted that the stiffness of the discretized model is expressed as the summation of four contributions so that all the stiffening terms resulting from the present consistent linearization are explicitly outlined and the effect of discarding one contribution can be easily studied by dropping the related quantity in the summation. For the sake of clarity, the four elastic terms in Eq. (56) are indicated as linear (L), geometric ($\mathrm{G_1}$ and $\mathrm{G_2}$), and centrifugal softening (Ω). If the gyroscopic coupling is assumed negligible and ignored, as done in some previous studies, the four set of equations can be solved separately.

7. Numerical analysis

In this section, the quadratic eigenvalue problems resulting from Eqs. (56) after assuming harmonic motion are solved to compute the natural frequencies of prismatic rotating beams made of isotropic material ($E/G = 2.6$). Some benchmark cases are selected with the aim of comparing the present model with the results available in the reference literature, so that the relevant differences with other modeling techniques can be outlined. Unless otherwise stated, beams having $J_3 = J_2$ are considered. A dimensionless parameter $\alpha = \sqrt{A\ell^2/J_3}$ is also introduced to represent the slenderness ratio of the beam. For the sake of comparison with previous studies, the following parameters are used for the angular velocity and natural frequencies:

$$\hat{\Omega} = \Omega T \qquad \lambda = \omega T \tag{57}$$

where T can take one of the following values

$$T_1 = \sqrt{\frac{\rho\ell^2}{E}} \qquad \text{or} \qquad T_2 = \sqrt{\frac{m\ell^4}{EJ_3}} = \alpha T_1 \tag{58}$$

as specified in each case under study.

7.1. Convergence analysis

A preliminary and comprehensive convergence study of the Ritz-Galerkin discretization applied to the present model was first carried out. In the following, two representative results are shown, where all the stiffening terms in Eqs. (56) are included in the analysis.

Table 1: Convergence study of the first five flapwise/torsional dimensionless frequencies.

		$\hat{\Omega}=10,\ \delta=0.1,\ \alpha=70$					$\hat{\Omega}=\hat{\Omega}_{\max},\ \delta=0.5,\ \alpha=100$				
$N_{\rm w}$	N_ϕ	1	2	3	4	5	1	2	3	4	5
1	1	13.0758	75.9610	–	–	–	21.3635	109.047	–	–	–
2	2	12.1785	44.0230	69.3903	247.726	–	20.2149	57.7876	99.8182	709.072	–
3	3	11.9647	34.9618	69.1141	123.308	212.355	19.8697	51.3276	99.4030	137.039	305.131
4	4	11.9113	34.9153	69.1049	76.7808	207.214	19.7184	51.3150	98.7422	99.4933	291.632
5	5	11.9017	34.9151	69.1042	76.7805	141.031	19.6711	51.2107	98.5745	99.4802	167.403
6	6	11.9006	34.8896	69.1040	76.0159	141.013	19.6590	51.1140	98.4336	99.4648	166.740
7	7	11.9005	34.8895	69.1039	75.9488	135.560	19.6560	51.1124	98.1454	99.4495	163.400
8	8	11.9005	34.8895	69.1039	75.9438	135.435	19.6555	51.1092	98.1453	99.4495	162.724
9	9	11.9005	34.8895	69.1039	75.9436	135.310	19.6554	51.1090	98.1451	99.4495	162.683
10	10	11.9005	34.8895	69.1039	75.9436	135.308	19.6554	51.1089	98.1447	99.4495	162.675
11	11	11.9005	34.8895	69.1039	75.9436	135.307	19.6554	51.1089	98.1447	99.4495	162.674
12	12	11.9005	34.8895	69.1039	75.9436	135.307	19.6554	51.1089	98.1447	99.4495	162.674
11	6	11.9005	34.8895	69.1039	75.9436	135.307	19.6554	51.1089	98.1447	99.4495	162.674

The first case is referred to the computation of the dimensionless natural frequencies $\lambda_i = \omega_i T_2$ of the coupled flapwise/torsional motion of rotating beams at a fixed angular velocity $\hat{\Omega} = \Omega T_2$, as the number $N_{\rm w}$, N_ϕ of admissible functions is increased. Table 1 presents the convergence properties of the first five frequency parameters computed using the following set of admissible functions

$$\Phi_{{\rm w}n}(x) = \left(\frac{x}{\ell}\right)^{n+1} \qquad \Phi_{\phi s}(x) = \left(\frac{x}{\ell}\right)^{s} \tag{59}$$

In particular, the results are listed for two different hub/beam systems. The first system is characterized by a hub radius ratio $\delta = 0.1$ and a slenderness ratio $\alpha = 70$, and is rotating at an angular velocity $\hat{\Omega} = 10$. According to the discussion in Section 3, this angular speed can be considered to be relatively high, as it corresponds to an equilibrium stretch at the root given by

$$\bar{e}_{root} = \frac{\hat{\Omega}^2}{\alpha^2}\,(\delta + 0.5) \approx 1.2\% \tag{60}$$

The second analysis is referred to a hub/beam system with $\delta = 0.5$ and $\alpha = 100$, rotating at the limiting angular speed corresponding to a maximum root strain of 2% given by

$$\hat{\Omega}_{\max} = \alpha\sqrt{\frac{0.02}{\delta + 0.5}} \approx 14.1 \tag{61}$$

For both configurations, Table 1 shows that the modal parameters converge monotonically from above to stable values as the number of terms in the Ritz series increases. It is observed that the convergence rate is rather high for the beam rotating at $\hat{\Omega} = 10$. Indeed, convergent values to five digits are obtained when $(N_{\rm w}, N_\phi) = (9, 9)$. It can be also noted that increasing the number of terms in the expansion of the twisting angle beyond a certain limit has very little effect on the converged frequencies. For example, no difference

can be appreciated in the first six digits of the computed results when $N_{\rm w} = 11$ and N_ϕ is increased from 6 to 11. This is due to the fact that the low-frequency response of the beam under study is dominated by the flexural behavior.

The rate of convergence for the second hub/beam system is slightly reduced with respect to the first case. This behavior could be induced by the increased angular velocity. When the angular speed is very large, bending curvatures measures at the root of the beam become quite large in the mode shapes dominated by bending. Indeed, in the theoretical limit as the angular speed approaches infinity, the local curvature at the beam root also approaches infinity. As observed by Peters [27], this means that Eq. (52) is reducing from a fourth-order to a second-order equation, so that the power series approximation in Eq. (59) becomes no more applicable, and convergence difficulties may arise. A measure of this phenomenon can be provided by evaluating the following bending stiffness parameter

$$\eta = \frac{EJ_3}{\bar{\nu}^2 m \ell^4 \Omega^2} \tag{62}$$

which multiplies the fourth-order derivative in Eq. (52) if it is written in a non-dimensional form. When η approaches zero, the flapwise equation approaches a second-order equation. Using Eq. (60), it can be seen that

$$\eta \approx O\left(\frac{1}{\bar{e}_{root}\alpha^2}\right) \tag{63}$$

Therefore, since the maximum strain root is limited in this study to 0.02 as discussed in Section 3, η could become very small for beams having very large slenderness ratio. The value selected for the second case analyzed in Table 1 ($\alpha = 100$) is not large enough to affect significantly the convergence rate. All the examples considered in this work will have limited values of α so that convergence difficulties can be avoided. For further details about convergence issues of Ritz-Galerkin approximation for rapidly rotating beams and discussion on possible remedies, the reader is referred to the work of Peters [27].

In the second case selected to show the convergence properties of the Ritz-Galerkin approximation, the analysis is focused on the coupled axial/chordwise frequencies. Results are shown in Table 2 for the first five frequency parameters $\lambda_i = \omega_i T_1$ of a beam with $\delta = 0$, $\alpha = 50$, rotating at $\hat{\Omega} = \Omega T_1 = 0.1$ ($\bar{e}_{root} = 0.005$) and a beam with $\delta = 0.5$, $\alpha = 150$, rotating at $\hat{\Omega} = \hat{\Omega}_{\rm max}$. The converged frequencies for different pairs ($N_{\rm u}$, $N_{\rm v}$) are evaluated by assuming again a power series approximation, i.e.,

$$\Phi_{{\rm u}j}(x) = \left(\frac{x}{\ell}\right)^j \qquad \Phi_{{\rm v}l}(x) = \left(\frac{x}{\ell}\right)^{l+1} \tag{64}$$

Similarly to the flapwise/torsional behavior, the convergence is monotonic from above and the rate of convergence is relatively high. Due to the dominance of the bending effect in the low-frequency range, the number of Ritz terms related to the longitudinal displacement can be relatively low compared to the expansion of the transverse motion in order to achieve a satisfactory convergence. Finally, the behavior is again affected by the angular velocity as observed in the flapwise/torsional case. However, even though a

Table 2: Convergence study of the first five axial/chordwise dimensionless frequencies.

		$\hat{\Omega}=0.1$, $\delta=0$, $\alpha=50$					$\hat{\Omega}=\hat{\Omega}_{\max}$, $\delta=0.5$, $\alpha=150$				
N_{u}	N_{v}	1	2	3	4	5	1	2	3	4	5
1	1	0.1060	1.7486	–	–	–	0.1549	1.7780	–	–	–
2	2	0.0836	0.7266	1.5965	5.6915	–	0.1394	0.4971	1.6325	5.7337	–
3	3	0.0814	0.4988	1.5906	2.3130	4.8660	0.1341	0.4638	1.0509	1.6263	4.9380
4	4	0.0812	0.4974	1.3090	1.5906	4.7515	0.1314	0.4635	0.8557	1.6263	2.0843
5	5	0.0812	0.4962	1.3081	1.5906	2.5583	0.1303	0.4605	0.8514	1.3740	1.6264
6	6	0.0812	0.4961	1.2827	1.5906	2.5579	0.1299	0.4594	0.8511	1.3576	1.6264
7	7	0.0812	0.4961	1.2825	1.5906	2.4290	0.1298	0.4593	0.8475	1.3507	1.6264
8	8	0.0812	0.4961	1.2825	1.5906	2.4286	0.1297	0.4591	0.8475	1.3405	1.6264
9	9	0.0812	0.4961	1.2825	1.5906	2.4250	0.1297	0.4591	0.8474	1.3405	1.6264
10	10	0.0812	0.4961	1.2825	1.5906	2.4250	0.1297	0.4591	0.8473	1.3404	1.6264
11	11	0.0812	0.4961	1.2825	1.5906	2.4250	0.1297	0.4591	0.8473	1.3404	1.6264
6	11	0.0812	0.4961	1.2823	1.5906	2.4250	0.1297	0.4591	0.8473	1.3404	1.6264

Table 3: Comparison of natural frequencies of a beam with $R=0.2$ m, $A=0.005\times0.05$ m^2, $\ell=2$ m, made of isotropic material with $E=70GPa$, $G=26GPa$, $\rho=2700\,kg/m^3$, and rotating at $\Omega=1000$ rpm.

	Flapwise		Chordwise		Torsional		Axial	
λ	Present	Ref. [17]	Present	Ref. [17]	Present	Ref. [17]	Present	Ref. [17]
1	114.13	114.10	87.44	87.25	2442.22	2439.42	4008.30	4003.18
2	279.59	279.54	482.88	481.39	7319.00	7312.39	12010.60	11998.51
3	460.15	460.10	1221.37	1213.14	12197.31	12186.54	20015.80	19996.08

very slender ($\alpha=150$) and rapidly rotating beam is considered, convergent values to five digits are obtained with $(N_{\mathrm{u}},\,N_{\mathrm{v}})=(10,10)$.

Based on the present convergence analysis, in the following numerical studies a number of terms $N=11$ is assumed for all the unknowns of the problem.

7.2. Comparison study

A comparison of the results from the present formulation with some benchmark cases available in the literature is provided in this section.

The first comparison is reported in Table 3, in which values of the natural frequencies obtained with the present theory are compared with those of another GEBT developed in Ref. [17] for an isotropic beam of length $\ell=2$ m, rectangular cross section $A=0.005\times0.05$ m^2 and rotating at $\Omega=1000$ rpm. The beam is attached to a rigid hub of radius $R=0.2$ m. It is seen that the agreement is very good. The results of the present approach are always slightly higher than those computed by Lacarbonara et al. [17]. This negligible discrepancy could be due to the different choice of the shape functions employed rather than to the additional stiffening terms present in the current formulation, since the angular velocity of the example,

Table 4: Comparison of the first and second dimensionless frequencies of the flapwise motion of a beam with $\delta = 0$ and $\alpha = 70$, rotating at different angular velocities $\hat{\Omega}$.

	λ_1			λ_2		
$\hat{\Omega}$	Present	Present (w/o rotary inertia)	Yoo and Shin [36]	Present	Present (w/o rotary inertia)	Yoo and Shin [36]
0	3.5143	3.5160	3.5160	21.962	22.035	22.035
1	3.6800	3.6818	3.6816	22.109	22.182	22.181
2	4.1357	4.1381	4.1373	22.543	22.619	22.615
3	4.7961	4.7992	4.7973	23.250	23.329	23.320
4	5.5851	5.5889	5.5850	24.205	24.289	24.273
5	6.4519	6.4564	6.4495	25.382	25.471	25.446
6	7.3663	7.3716	7.3604	26.751	26.847	26.809
7	8.3107	8.3167	8.2996	28.290	28.388	28.334
8	9.2749	9.2815	9.2568	29.960	30.070	29.995
9	10.253	10.260	10.226	31.871	31.726	31.771
10	11.241	11.249	11.202	33.642	33.771	33.640

corresponding to an equilibrium root strain $\bar{e}_{root} \approx 0.1\%$, can be considered to be relatively low.

Table 4 shows the first and second nondimensional frequencies $\lambda_i = \omega_i T_2$ for the flapwise vibrations of a rotating beam with slenderness ratio $\alpha = 70$. The hub radius ratio δ is set to zero and the natural frequencies are listed for different angular velocities $\hat{\Omega} = \Omega T_2$. Present computations are obtained with admissible functions given by Eq. (59) and compared with those obtained by Yoo and Shin [36] using the foreshortening approach. It is observed that the frequency values show some differences compared to Ref. [36]. This is due to the fact that the formulation in Yoo and Shin [36] neglects the gyroscopic coupling with the torsional motion, the effect of rotary inertia and the geometric stiffness contribution arising from $\delta W_i^{(G_2)}$ associated with the consistent linearization about the deformed equilibrium configuration of the rotating beam. The influence of rotary inertia could be evaluated from the results in Table 4 computed using the present theory without rotary inertia. In this case, it is noted that the present values are very close to those listed by Yoo and Shin [36], especially when the angular velocity is small. Instead, the discrepancy between the two approaches becomes larger if all dynamic terms are retained in the present formulation and the angular speed of the beam increases. This is due to the increasing contribution of the gyroscopic terms and additional stiffening effects.

Another comparison is reported in Table 5, where the first six coupled axial/chordwise natural frequencies $\lambda_i = \omega_i T_1$ of a rotating hub/beam system with various hub radius ratios δ and slenderness ratios α are shown for two different angular velocities $\hat{\Omega} = \Omega T_1 = 0.01$ and 0.06. Present computations obtained using the full model in Eqs. (56) are compared with the results of Huang et al. [13], whose model has the same inertial contributions but it is based on Von-Karman strains. It is observed that when $\hat{\Omega} = 0.01$ the natural frequencies corresponding to the formulation proposed here are in very good agreement with Ref. [13] for

Table 5: Comparison of the first six axial/chordwise dimensionless frequencies of rotating beams with different δ, α and $\hat{\Omega}$ values.

				λ					
δ	$\hat{\Omega}$	α	Method	1	2	3	4	5	6
0	0.01	50	Present	0.07039	0.43848	1.21599	1.57100	2.35250	3.82718
			Huang et al. [13]	0.07039	0.43847	1.21597	1.57089	2.35246	3.82715
		100	Present	0.03542	0.22123	0.61597	1.20193	1.57099	1.97771
			Huang et al. [13]	0.03542	0.22122	0.61596	1.20191	1.57089	1.97766
	0.06	50	Present	0.07470	0.45965	1.23982	1.57795	2.37837	3.85457
			Huang et al. [13]	0.07461	0.45936	1.23905	1.57427	2.37684	3.85195
		100	Present	0.04260	0.26094	0.66189	1.25174	1.57793	2.02980
			Huang et al. [13]	0.04251	0.26077	0.66148	1.25097	1.57425	2.02856
1.5	0.01	50	Present	0.07204	0.43995	1.21753	1.57124	2.35415	3.82901
			Huang et al. [13]	0.07204	0.43993	1.21746	1.57089	2.35401	3.82873
		100	Present	0.03860	0.22414	0.61900	1.20513	1.57124	1.98102
			Huang et al. [13]	0.03860	0.22413	0.61896	1.20507	1.57089	1.98091
	0.06	50	Present	0.11802	0.50769	1.29272	1.58684	2.43605	3.91594
			Huang et al. [13]	0.11784	0.50687	1.29036	1.57429	2.43127	3.90780
		100	Present	0.10002	0.33764	0.75474	1.35658	1.58682	2.14236
			Huang et al. [13]	0.09989	0.33722	0.75363	1.35435	1.57427	2.13860

both $\alpha = 50$ and $\alpha = 100$ and for any value of the hub radius ratio δ. As already outlined in the previous example, the difference between the two approaches increases when $\hat{\Omega} = 0.06$. In particular, the present frequency values are higher than those computed by Huang et al. [13], due to the stiffening effects included in the present formulation.

In order to point out more clearly the importance of a fully consistent linearization for accurate vibration analysis of rapidly rotating beams, the following example involving angular speeds higher than those assumed in the previous case is presented and discussed. The analysis is reported in Table 6, where the fundamental axial/chordwise frequency $\lambda = \omega T_1$ computed with the present theory is compared with the reference results

Table 6: Comparison of the fundamental axial/chordwise dimensionless frequency of a beam with $\delta = 0$ and $\alpha = 100$, rotating at different angular velocities.

$\hat{\Omega}$	Present (no rotary inertia)	Present (Von-Karman)	Banerjee and Kennedy [3]	$\Delta\%$
0.05	0.04071	0.04066	0.04066	0.1
0.10	0.05060	0.05010	0.05010	1.0
0.12	0.05459	0.05367	–	1.7
0.14	0.05855	0.05701	–	2.7
0.16	0.06253	0.06011	–	4.0
0.18	0.06657	0.06300	–	5.7
0.20	0.07073	0.06568	–	7.7

provided by Banerjee and Kennedy [3] for a beam with slenderness ratio $\alpha = 100$ and different values of $\hat{\Omega} = \Omega T_1$. Note that the limit value of the angular speed $\hat{\Omega}$ where the equilibrium state is still characterized by linear strains is equal to 0.2 for the case under study. Since an Euler-Bernoulli beam model is assumed in Ref. [3], for the sake of comparison frequency results are computed by deleting all terms related to rotary inertia in the present model. The corresponding values are shown in the second column of Table 6. In addition to neglecting the effect of rotary inertia, the von-Karman based equations developed by Banerjee and Kennedy [3] can be derived from the present formulation by discarding the stiffening terms arising from linearization about the deformed equilibrium condition. The related results are shown in the third column of Table 6. Finally, the percentage difference Δ between the frequency values of the full model without rotary inertia and the model based on von-Karman nonlinearities is reported in the last column of Table 6. It is first observed that the results in Ref. [3] for $\hat{\Omega} = 0.05$ and 0.1 are exactly obtained. This means that the von-Karman-like model derived from the present full model under the assumptions explained before can be used to provide reference solutions also for those values of the angular velocity ($\hat{\Omega}$ from 0.12 to 0.2) not reported by Banerjee and Kennedy [3]. It is evident that the percentage difference Δ increases as the angular velocity increases and is significant when $\hat{\Omega}$ is close to the limit of validity of the present formulation. As expected, present results are always higher than those of Banerjee and Kennedy [3] due the effect of the axial stiffening. Indeed, since the axial and chordwise vibrations are coupled through the Coriolis terms and the gyroscopic coupling is proportional to the angular velocity, a partially consistent representation of the linearized axial stiffness will affect the in-plane lateral vibrations of beams rotating at high angular velocity.

7.3. Variation with angular velocity

A closer look at Tables 4 to 6 shows that the natural frequencies of the rotating beam obtained from the present computations increase with increasing values of the rotating velocity for all cases considered in the previous comparison studies. Due to the presence of the centrifugal softening terms in the equations of motion, one might wonder whether the above observation has a general validity or the present linearized model exhibits a divergence instability at a critical value of Ω. Indeed, some models available in the literature (see, for example, the works of Yoo and Shin [36] and Banerjee and Kennedy [3]) predict a trend where the fundamental frequency of the beam in chordwise motion first increases as Ω increases until it reaches a peak value and then gradually decreases and becomes zero at a critical value of the angular velocity. This phenomenon was explained by Hodges and Bless [8] as a consequence of adopting linear strains well beyond the validity range of the linear behavior of common engineering materials. According to what shown in this work, the prediction of instability can be also attributed to the lacking of axial stiffening as a result of the use of Von-Karman strains as a deformation measure.

The variation of the first four dimensionless flapwise/torsional frequencies $\lambda_i = \omega_i T_2$ as a function of the dimensionless angular velocity $\hat{\Omega} = \Omega T_2$ is depicted in Figure 6 for a beam with $\delta = 0$ and different

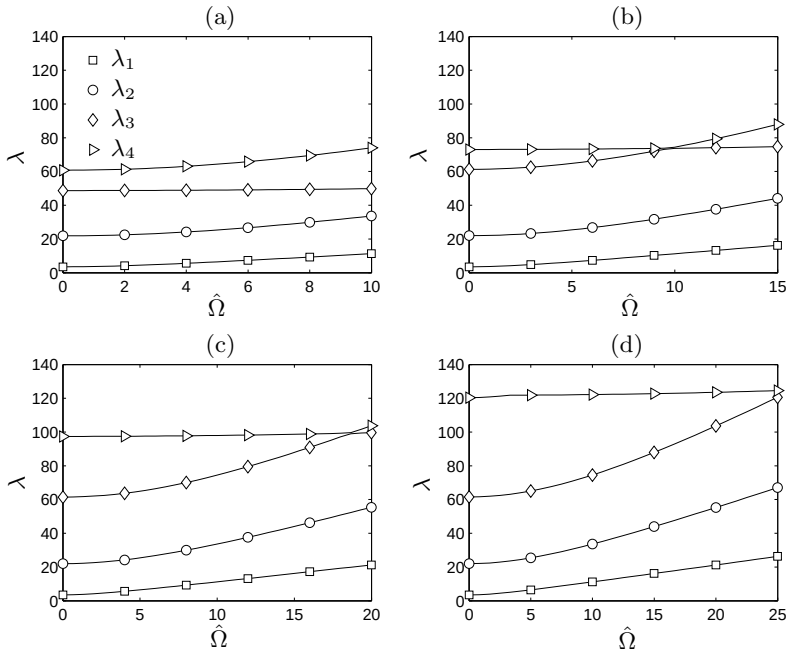

Figure 6: Variation of the flapwise/torsional frequencies with the rotational speed $\hat{\Omega}$. (a) $\alpha = 50$; (b) $\alpha = 75$; (c) $\alpha = 100$; (d) $\alpha = 125$.

slenderness ratio ($\alpha = 50, 75, 100, 125$). $\hat{\Omega}$ varies from zero to its maximum admissible value for each case, thus encompassing the whole range of validity of the model. It is worth noting that the conclusions which can be drawn from this analysis are considered rather confident since the curves in Fig. 6 cover a wide spectrum of practical cases where the present model can be applied. Furthermore, the behavior in Fig. 6 is obtained for $\delta = 0$, which corresponds to the lowest value of the stiffening terms due to the geometric effects. As a result, if no instability occurs in this case, it can be argued that the model is also stable for positive values of δ since the beam would be stiffer. It is observed that all the frequencies monotonically increase with increasing rotational speed. Therefore, it can be said that the centrifugal softening terms in the equations of motion are correctly compensated by the geometric stiffening. It is also worth noting that there is a strong interaction between some modes, which results in veering/crossing regions.

A numerical study similar to that shown in Fig. 6 was also carried out for coupled axial/chordwise vibrations. Figure 7 shows the first four natural frequencies $\lambda_i = \omega_i T_1$ of a beam with $\delta = 0$ and $\alpha = 50, 75, 100$ and 125, rotating at angular velocity $\hat{\Omega} = \Omega T_1$ going from zero to $\hat{\Omega}_{\max}$. Similarly to the previous case, it is clear from Fig. 7 that, within its range of validity, the present model predicts increasing axial/chordwise natural frequencies as the angular velocity of the hub increases.

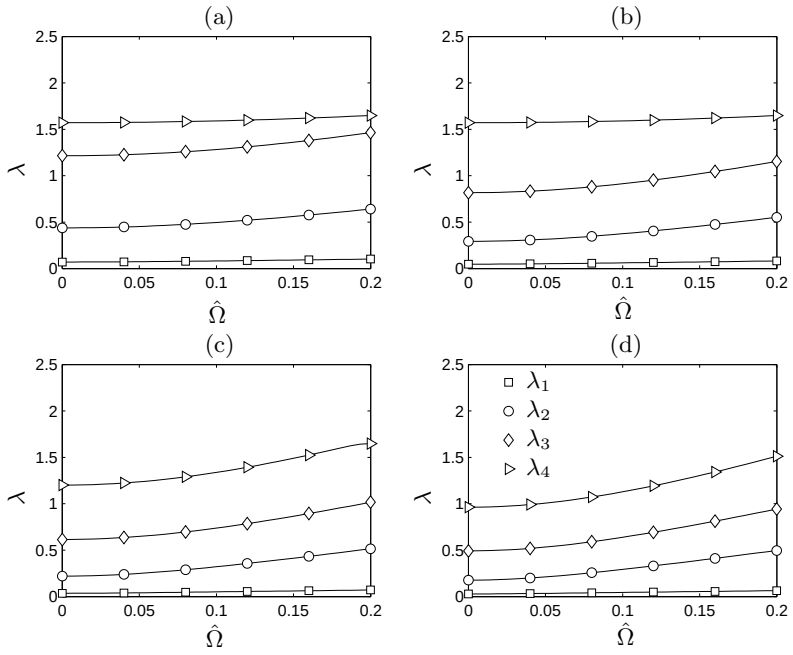

Figure 7: Variation of the axial/chordwise frequencies with the rotational speed $\hat{\Omega}$. (a) $\alpha = 50$; (b) $\alpha = 75$; (c) $\alpha = 100$; (d) $\alpha = 125$.

7.4. Influence of the equilibrium configuration

Since the main difference between the present formulation and other approaches relies on the fully consistent linearization about the deformed equilibrium configuration, the influence of the related stiffening terms on the natural frequencies of the rotating beam is here specifically underlined. In particular, the analysis is focused on the axial/chordwise vibrations, with the aim of evaluating the effect of the axial stiffening. Indeed, when the angular velocity Ω is small, the axial deformation of the equilibrium configuration can be assumed infinitesimal and a linearization about the undeformed configuration appears a reasonable approximation. However, when the undeformed configuration is used, the geometric stiffening terms due to the pre-deformation effect are completely discarded and the geometric stiffness is computed without the contribution of the equilibrium axial displacement. It is shown in the following that this classical approximation could lead to relevant inaccuracy of the vibration response when the angular speed takes high values.

Table 7 is referred to a beam with $\delta = 0$ and $\alpha = 70$, rotating at different velocities up to $\hat{\Omega} = \hat{\Omega}_{\max}$, where $\hat{\Omega}_{\max}$ is evaluated from Eq. (31), as usual. The first frequency parameter $\lambda_1 = \omega_1 T_1$ is reported as computed from a linearized model about undeformed and deformed equilibrium configuration, respectively. It is shown that the model linearized about the deformed geometry of the beam provides higher values. The difference is negligible when $\hat{\Omega}/\hat{\Omega}_{\max} = 0.1$ but increases as the angular velocity approaches its maximum value. It is worth noting that, in this limiting condition, the modeling error introduced by taking the

Table 7: Fundamental chordwise dimensionless frequency of a rotating beam with $\delta = 0$ and $\alpha = 70$. Comparison between models linearized about the undeformed and deformed equilibrium configuration.

	Configuration		
$\hat{\Omega}/\hat{\Omega}_{\max}$	Undeformed	Deformed	$\Delta\%$
0.10	0.0509	0.0509	0.0
0.25	0.0544	0.0545	0.2
0.50	0.0633	0.0636	0.5
0.75	0.0725	0.0739	1.9
1.00	0.0806	0.0846	5.0

Table 8: Fundamental chordwise dimensionless frequency of beams with $\delta = 0$ and various slenderness ratios α, rotating at $\hat{\Omega} = \hat{\Omega}_{\max}$. Comparison between models linearized about the undeformed and deformed equilibrium configuration.

	Configuration		
α	Undeformed	Deformed	$\Delta\%$
50	0.0985	0.1018	3.4
75	0.0775	0.0816	5.3
100	0.0660	0.0707	7.1
125	0.0585	0.0637	8.9
150	0.0531	0.0587	10.5

undeformed geometry as the equilibrium configuration can be as high as 5%.

The effect of the deformed/undeformed equilibrium configuration on the estimation of the beam vibrations is also studied in Table 8 as a function of the slenderness ratio α. The beam is rotating at $\hat{\Omega} = \hat{\Omega}_{\max}$. It is observed that an increment of α results in an increasing difference between the two models. This could be explained by the larger axial deformation induced by the rotation when the beam becomes slender. A significant discrepancy of about 10% is obtained for the fundamental lateral mode when $\alpha = 150$. Therefore, it appears that including all the stiffening terms arising from a fully consistent linearization is crucial to obtain accurate estimation of the chordwise natural frequencies for rapidly rotating beams with high slenderness ratios.

8. Conclusions

This paper has presented a fully consistent linearized model suitable for accurate free vibration analysis of prismatic beams rotating in a plane at constant angular velocity. The equations of motion are derived within the framework of the geometrically exact beam theory. Second-order generalized strains are properly taken into account in the linearization process. As a result, some non-classical geometric stiffening terms appear in the governing equations, whose effect in the vibration response was studied by an approximate solution based on a Ritz-Galerkin discretization.

The differences among the present approach and some closely related models available in the literature have been pointed out both theoretically and through a comprehensive numerical analysis involving beams with various hub radius ratios and slenderness ratios. The additional stiffening contributions arising from the tension induced by the centrifugal forces have been extensively discussed. In particular, models which neglect second-order generalized terms prior to the linearization tend to underestimate the natural frequencies, as confirmed by several numerical examples and comparisons. The difference can be significant when the beam is rotating at very high angular velocity, still within the limit of a physically linear constitutive law. Finally, a numerical analysis has shown that discarding completely the geometric stiffness contribution due to the pre-deformation effect in the axial/chordwise equations could strongly affect the accuracy of the computed frequencies, in particular for high values of the slenderness ratio of the beam.

Acknowledgments

The authors would like to thank the Editor and the anonymous reviewers for their constructive and valuable suggestions.

Appendix A

In the linearized set of Eq. (56), the elements of the mass matrices are given by

$$M_{ij}^{\mathrm{uu}} = m\int_0^\ell \Phi_{\mathrm{u}i}\Phi_{\mathrm{u}j}\mathrm{d}x \qquad M_{kl}^{\mathrm{vv}} = m\int_0^\ell \Phi_{\mathrm{v}k}\Phi_{\mathrm{v}l}\mathrm{d}x + I_3\int_0^\ell \frac{1}{\bar{\nu}^2}\frac{\mathrm{d}\Phi_{\mathrm{v}k}}{\mathrm{d}x}\frac{\mathrm{d}\Phi_{\mathrm{v}l}}{\mathrm{d}x}\mathrm{d}x \tag{65}$$

$$M_{mn}^{\mathrm{ww}} = m\int_0^\ell \Phi_{\mathrm{w}m}\Phi_{\mathrm{w}n}\mathrm{d}x + I_2\int_0^\ell \frac{1}{\bar{\nu}^2}\frac{\mathrm{d}\Phi_{\mathrm{w}m}}{\mathrm{d}x}\frac{\mathrm{d}\Phi_{\mathrm{w}n}}{\mathrm{d}x}\mathrm{d}x \qquad M_{rp}^{\phi\phi} = I_1\int_0^\ell \Phi_{\phi r}\Phi_{\phi p}\mathrm{d}x \tag{66}$$

The gyroscopic elements corresponding to Coriolis force terms are written as

$$G_{il}^{\mathrm{uv}} = 2m\Omega\int_0^\ell \Phi_{\mathrm{u}i}\Phi_{\mathrm{v}l}\mathrm{d}x \qquad G_{kj}^{\mathrm{vu}} = 2m\Omega\int_0^\ell \Phi_{\mathrm{v}k}\Phi_{\mathrm{u}j}\mathrm{d}x \tag{67}$$

$$G_{mp}^{\mathrm{w}\phi} = 2I_2\Omega\int_0^\ell \frac{1}{\bar{\nu}}\frac{\mathrm{d}\Phi_{\mathrm{w}m}}{\mathrm{d}x}\Phi_{\phi p}\mathrm{d}x \qquad G_{rn}^{\phi\mathrm{w}} = 2I_2\Omega\int_0^\ell \frac{1}{\bar{\nu}}\Phi_{\phi r}\frac{\mathrm{d}\Phi_{\mathrm{w}n}}{\mathrm{d}x}\mathrm{d}x \tag{68}$$

The linear stiffening terms are given by the classical quantities of linear elasticity for slender beams as follows

$$K_{ij}^{\mathrm{uu(L)}} = EA\int_0^\ell \frac{\mathrm{d}\Phi_{\mathrm{u}i}}{\mathrm{d}x}\frac{\mathrm{d}\Phi_{\mathrm{u}j}}{\mathrm{d}x}\mathrm{d}x \qquad K_{kl}^{\mathrm{vv(L)}} = EJ_3\int_0^\ell \frac{1}{\bar{\nu}^2}\frac{\mathrm{d}^2\Phi_{\mathrm{v}k}}{\mathrm{d}x^2}\frac{\mathrm{d}^2\Phi_{\mathrm{v}l}}{\mathrm{d}x^2}\mathrm{d}x \tag{69}$$

$$K_{mn}^{\mathrm{ww(L)}} = EJ_2\int_0^\ell \frac{1}{\bar{\nu}^2}\frac{\mathrm{d}^2\Phi_{\mathrm{w}m}}{\mathrm{d}x^2}\frac{\mathrm{d}^2\Phi_{\mathrm{w}n}}{\mathrm{d}x^2}\mathrm{d}x \qquad K_{rp}^{\phi\phi\mathrm{(L)}} = GJ\int_0^\ell \frac{\mathrm{d}\Phi_{\phi r}}{\mathrm{d}x}\frac{\mathrm{d}\Phi_{\phi p}}{\mathrm{d}x}\mathrm{d}x \tag{70}$$

The centrifugal softening stiffness is expressed through the following contributions

$$K_{ij}^{\mathrm{uu}(\Omega)} = m\Omega^2\int_0^\ell \Phi_{\mathrm{u}i}\Phi_{\mathrm{u}j}\mathrm{d}x \qquad K_{kl}^{\mathrm{vv}(\Omega)} = m\Omega^2\int_0^\ell \Phi_{\mathrm{v}k}\Phi_{\mathrm{v}l}\mathrm{d}x \tag{71}$$

$$K_{mn}^{\mathrm{ww}(\Omega)} = I_2\Omega^2 \int_0^\ell \frac{1}{\bar{\nu}^2}\frac{\mathrm{d}\Phi_{\mathrm{w}m}}{\mathrm{d}x}\frac{\mathrm{d}\Phi_{\mathrm{w}n}}{\mathrm{d}x}\mathrm{d}x \qquad K_{rp}^{\phi\phi(\Omega)} = (I_2 - I_3)\,\Omega^2 \int_0^\ell \Phi_{\phi r}\Phi_{\phi p}\mathrm{d}x \tag{72}$$

The geometric stiffening terms are given by

$$K_{ij}^{\mathrm{uu}(\mathrm{G}_1)} = \int_0^\ell \bar{\sigma}_{11} A \frac{\mathrm{d}\Phi_{\mathrm{u}i}}{\mathrm{d}x}\frac{\mathrm{d}\Phi_{\mathrm{u}j}}{\mathrm{d}x}\mathrm{d}x \qquad K_{kl}^{\mathrm{vv}(\mathrm{G}_1)} = \int_0^\ell \bar{N}\frac{\mathrm{d}\Phi_{\mathrm{v}k}}{\mathrm{d}x}\frac{\mathrm{d}\Phi_{\mathrm{v}l}}{\mathrm{d}x}\mathrm{d}x + J_3\int_0^\ell \frac{\bar{\sigma}_{11}}{\bar{\nu}^2}\frac{\mathrm{d}^2\Phi_{\mathrm{v}k}}{\mathrm{d}x^2}\frac{\mathrm{d}^2\Phi_{\mathrm{v}l}}{\mathrm{d}x^2}\mathrm{d}x \tag{73}$$

$$K_{mn}^{\mathrm{ww}(\mathrm{G}_1)} = \int_0^\ell \bar{N}\frac{\mathrm{d}\Phi_{\mathrm{w}m}}{\mathrm{d}x}\frac{\mathrm{d}\Phi_{\mathrm{w}n}}{\mathrm{d}x}\mathrm{d}x + J_2\int_0^\ell \frac{\bar{\sigma}_{11}}{\bar{\nu}^2}\frac{\mathrm{d}^2\Phi_{\mathrm{w}m}}{\mathrm{d}x^2}\frac{\mathrm{d}^2\Phi_{\mathrm{w}n}}{\mathrm{d}x^2}\mathrm{d}x \qquad K_{rp}^{\phi\phi(\mathrm{G}_1)} = \int_0^\ell \bar{\sigma}_{11} J_1 \frac{\mathrm{d}\Phi_{\phi r}}{\mathrm{d}x}\frac{\mathrm{d}\Phi_{\phi p}}{\mathrm{d}x}\mathrm{d}x \tag{74}$$

$$K_{ij}^{\mathrm{uu}(\mathrm{G}_2)} = 2\int_0^\ell \bar{\sigma}_{11} A \frac{\mathrm{d}\Phi_{\mathrm{u}i}}{\mathrm{d}x}\frac{\mathrm{d}\Phi_{\mathrm{u}j}}{\mathrm{d}x}\mathrm{d}x \qquad K_{kl}^{\mathrm{vv}(\mathrm{G}_2)} = 2J_3\int_0^\ell \frac{\bar{\sigma}_{11}}{\bar{\nu}^2}\frac{\mathrm{d}^2\Phi_{\mathrm{v}k}}{\mathrm{d}x^2}\frac{\mathrm{d}^2\Phi_{\mathrm{v}l}}{\mathrm{d}x^2}\mathrm{d}x \tag{75}$$

$$K_{mn}^{\mathrm{ww}(\mathrm{G}_2)} = 2J_2\int_0^\ell \frac{\bar{\sigma}_{11}}{\bar{\nu}^2}\frac{\mathrm{d}^2\Phi_{\mathrm{w}m}}{\mathrm{d}x^2}\frac{\mathrm{d}^2\Phi_{\mathrm{w}n}}{\mathrm{d}x^2}\mathrm{d}x \tag{76}$$

By using integration by parts, the integrals involving the stress $\bar{\sigma}_{11}$ at the equilibrium condition can be written in an alternative form which is of help in pointing out the effect of the hub radius R. Referring for example to the geometric stiffness $K_{ij}^{\mathrm{uu}(\mathrm{G}_1)}$, it can be rewritten as follows

$$\begin{aligned} K_{ij}^{\mathrm{uu}(\mathrm{G}_1)} &= \int_0^\ell \bar{\sigma}_{11} A \frac{\mathrm{d}\Phi_{\mathrm{u}i}}{\mathrm{d}x}\frac{\mathrm{d}\Phi_{\mathrm{u}j}}{\mathrm{d}x}\mathrm{d}x = \\ &= m\Omega^2 R\int_0^\ell\int_0^x \frac{\mathrm{d}\Phi_{\mathrm{u}i}}{\mathrm{d}\xi}\frac{\mathrm{d}\Phi_{\mathrm{u}j}}{\mathrm{d}\xi}\mathrm{d}\xi\mathrm{d}x + m\Omega^2\int_0^\ell (x+\bar{u})\int_0^x \frac{\mathrm{d}\Phi_{\mathrm{u}i}}{\mathrm{d}\xi}\frac{\mathrm{d}\Phi_{\mathrm{u}j}}{\mathrm{d}\xi}\mathrm{d}\xi\mathrm{d}x \end{aligned} \tag{77}$$

The other geometric stiffness quantities can be rearranged in a similar manner.

References

[1] Arvin, H., Lacarbonara, W., Mar 2014. A fully nonlinear dynamic formulation for rotating composite beams: Nonlinear normal modes in flapping. Composite Structures 109, 93–105.

[2] Banerjee, A. K., Dickens, J. M., 1990. Dynamics of an arbitrary flexible body in large rotation and translation. Journal of Guidance, Control, and Dynamics 13 (2), 221–227.

[3] Banerjee, J., Kennedy, D., 2014. Dynamic stiffness method for inplane free vibration of rotating beams including coriolis effects. Journal of Sound and Vibration 333 (26), 7299–7312.

[4] Borri, M., Merlini, T., 1986. A large displacement formulation for anisotropic beam analysis. Meccanica 21 (1), 30–37.

[5] Cardona, A., Geradin, M., 1988. A beam finite element non-linear theory with finite rotations. International journal for numerical methods in engineering 26 (11), 2403–2438.

[6] Danielson, D. A., Hodges, D. H., 1987. Nonlinear beam kinematics by decomposition of the rotation tensor. Journal of Applied Mechanics 54 (2), 258–262.

[7] Giurgiutiu, V., Stafford, R., 1977. Semi-analytic methods for frequencies and mode shapes of rotor blades. Vertica 1 (4), 291–306.

[8] Hodges, D., Bless, R., 1994. Axial instability of rotating rods revisited. International journal of non-linear mechanics 29 (6), 879–887.

[9] Hodges, D. H., 1990. A mixed variational formulation based on exact intrinsic equations for dynamics of moving beams. International journal of solids and structures 26 (11), 1253–1273.

[10] Hodges, D. H., 2006. Nonlinear Composite Beam Theory. American Institute of Aeronautics and Astronautics (AIAA).

[11] Hodges, D. H., Rutkowski, M. Y., 1981. Free-vibration analysis of rotating beams by a variable-order finite-element method. AIAA Journal 19 (11), 1459–1466.

[12] Houbolt, J. C., Brooks, G. W., 1958. Differential equations of motion for combined flapwise bending, chordwise bending, and torsion of twisted nonuniform rotor blades. Tech. Rep. 1346, NACA.

[13] Huang, C. L., Lin, W. Y., Hsiao, K. M., Sep 2010. Free vibration analysis of rotating Euler beams at high angular velocity. Computers & Structures 88 (17-18), 991–1001.

[14] Kane, T., Ryan, R., Banerjee, A., 1987. Dynamics of a cantilever beam attached to a moving base. Journal of Guidance, Control, and Dynamics 10 (2), 139–151.

[15] Kim, H., Hee Yoo, H., Chung, J., Oct 2013. Dynamic model for free vibration and response analysis of rotating beams. Journal of Sound and Vibration 332 (22), 5917–5928.

[16] Kunz, D. L., 1994. Survey and comparison of engineering beam theories for helicopter rotor blades. Journal of Aircraft 31 (3), 473–479.

[17] Lacarbonara, W., Arvin, H., Bakhtiari-Nejad, F., Jun 2012. A geometrically exact approach to the overall dynamics of elastic rotating blades, part 1: linear modal properties. Nonlinear Dyn 70 (1), 659–675.

[18] Laskin, R., Likins, P., Longman, R., 1983. Dynamical equations of a free-free beam subject to large overall motions. Journal of the Austronautical Sciences 31, 507–528.

[19] Likins, P. W., Barbera, J., Baddeley, V., 1973. Mathematical modeling of spinning elastic bodies for modal analysis. AIAA journal 11 (9), 1251–1258.

[20] Lin, S., Hsiao, K., 2001. Vibration analysis of a rotating timoshenko beam. Journal of Sound and Vibration 240 (2), 303–322.

[21] Masarati, P., Morandini, M., 2002. On the modeling of rotating beams for rotorcraft blade analysis. In: 28th European Rotorcraft Forum. Citeseer, pp. 62–1.

[22] Mayo, J. M., Garcia-Vallejo, D., Dominguez, J., 2004. Study of the geometric stiffening effect: comparison of different formulations. Multibody System Dynamics 11 (4), 321–341.

[23] Meirovitch, L., 1991. Hybrid state equations of motion for flexible bodies in terms of quasi-coordinates. Journal of Guidance, Control, and Dynamics 14 (5), 1008–1013.

[24] Pai, P. F., 2007. Highly flexible structures: modeling, computation, and experimentation. AIAA (American Institute of Aeronautics & Ast.

[25] Pai, P. F., 2014. Problems in geometrically exact modeling of highly flexible beams. Thin-walled structures 76, 65–76.

[26] Pai, P. F., Qian, X., Du, X., Mar 2013. Modeling and dynamic characteristics of spinning Rayleigh beams. International Journal of Mechanical Sciences 68, 291–303.

[27] Peters, D. A., 1973. An approximate solution for the free vibrations of rotating uniform cantilever beams. NASA STI/Recon Technical Report N 78, 33289.

[28] Reissner, E., 1972. On one-dimensional finite-strain beam theory: the plane problem. Zeitschrift für angewandte Mathematik und Physik ZAMP 23 (5), 795–804.

[29] Reissner, E., Jun 1973. On one-dimensional large-displacement finite-strain beam theory. Studies in Applied Mathematics 52 (2), 87–95.

[30] Sharf, I., 1995. Geometric stiffening in multibody dynamics formulations. Journal of Guidance, Control, and Dynamics 18 (4), 882–890.

[31] Simo, J., 1985. A finite strain beam formulation. the three-dimensional dynamic problem. part i. Computer methods in applied mechanics and engineering 49 (1), 55–70.

[32] Stafford, R., Giurgiutiu, V., 1975. Semi-analytic methods for rotating timoshenko beams. International Journal of Mechanical Sciences 17 (11), 719–727.

[33] Vigneron, F., 1975. Comment on" mathematical modeling of spinning elastic bodies for modal analysis". AIAA Journal 13 (1), 126–127.

[34] Wright, A., Smith, C., Thresher, R., Wang, J., 1982. Vibration modes of centrifugally stiffened beams. Journal of Applied Mechanics 49 (1), 197–202.

[35] Yardimoglu, B., Inman, D. J., 2004. Coupled bending-bending-torsion vibration of a rotating pre-twisted beam with aerofoil cross-section and flexible root by finite element method. Shock and Vibration 11 (5-6), 637–646.

[36] Yoo, H., Shin, S., 1998. Vibration analysis of rotating cantilever beams. Journal of Sound and Vibration 212 (5), 807–828.